Assessment of uncertainty in river flow projections for the Mekong River using multiple GCMs and hydrological models

J.R. Thompson[a,*], A.J. Green[a], D.G. Kingston[b], S.N. Gosling[c]

a. Wetland Research Unit, UCL Department of Geography, University College London, Gower Street, London, UK, WC1E 6BT (j.r.thompson@ucl.ac.uk / amanda.green.09@ucl.ac.uk)

b. Department of Geography, University of Otago, PO Box 56, Dunedin, New Zealand (daniel.kingston@geography.otago.ac.nz)

c. School of Geography, The University of Nottingham, University Park, Nottingham, UK, NG7 2RD (simon.gosling@nottingham.ac.uk)

* Corresponding author: Email: j.r.thompson@ucl.ac.uk / Tel: +44 207 679 0589 / Fax: +44 0207 679 0565

Abstract

Hydrological model-related uncertainty is often ignored within climate change hydrological impact assessments. A MIKE SHE model is developed for the Mekong using the same data as an earlier semi-distributed, conceptual model (SLURP). The model is calibrated and validated using discharge at 12 gauging stations. Two sets of climate change scenarios are investigated. The first is based on a 2 °C increase in global mean temperature (the hypothesised threshold of 'dangerous' climate change), as simulated by seven GCMs. There are considerable differences in scenario discharge between GCMs, ranging from catchment-wide increases in mean discharge (up to 12.7%; CCCMA CGCM31, NCAR CCSM30), decreases (up to 21.6% in the upper catchments; CSIRO Mk30, IPSL CM4), and spatially varying responses (UKMO HadCM3 and HadGEM1, MPI ECHAM5). Inter-GCM differences are largely driven by differences in

precipitation. The second scenario set (HadCM3, increases in global mean temperature of 1–6 °C) shows consistently greater discharge (maximum: 28.7%) in the upper catchment as global temperature increases, primarily due to increasing precipitation. Further downstream, discharge is strongly influenced by increasing PET, which outweighs impacts of elevated upstream precipitation and causes consistent discharge reductions for higher temperatures (maximum: -5.3% for the main Mekong). MIKE SHE results for all scenarios are compared with those from the SLURP catchment model and the Mac-PDM.09 global hydrological model. Although hydrological model-related uncertainty is evident, its magnitude is smaller than that associated with choice of GCM. In most cases, the three hydrological models simulate the same direction of change in mean discharge. Mac-PDM.09 simulates the largest discharge increases when they occur, which is responsible for some differences in direction of change at downstream gauging stations for some scenarios, especially HadCM3. Inter-hydrological model differences are likely attributed to alternative model structures, process representations and PET methods (Linacre for MIKE SHE and SLURP, Penman-Monteith for Mac-PDM.09).

Keywords: Mekong, MIKE SHE, SLURP, Mac-PDM, climate change, uncertainty

1. Introduction

It is widely acknowledged that climate change will impact the global hydrological cycle (Kundzewicz *et al.*, 2007; Arnell and Gosling, 2013), with implications for human use of water resources (Bates *et al.*, 2008; Gosling *et al.*, 2011b; Gosling, 2012) and aquatic ecosystems (e.g. Poff *et al.*, 2002; Matthews and Quesne, 2009). Evaluation of the hydrological impacts of climate change is most commonly based upon driving a hydrological model with climatic projections derived from general circulation models (GCMs) forced with alternative emissions scenarios. This approach has been used in the assessment of climate change impacts for hydrological systems that vary in scale from small wetlands located within wider catchments (e.g. Thompson *et al.*, 2009), through small to medium sized catchments (e.g. Chun *et al.*, 2009; Thompson, 2012), major river basins (e.g. Conway and Hulme, 1996; Nijssen, 2001), to the national (e.g. Andréasson *et al.*, 2004), regional (e.g. Arnell, 1999a) and global scales (e.g. Arnell, 2003; Nohara, 2006; Gosling *et al.*, 2010).

There are a range of uncertainties that are introduced throughout these climate change hydrological impact assessments (Nawaz and Adeloye, 2006; Gosling *et al.*, 2011a). Uncertainty is firstly related to the definition of the greenhouse gas emissions scenarios used to force the GCMs. Secondly, uncertainty is associated with these GCMs, with climate model structural uncertainty causing different models to produce different climate projections for the same emissions scenario. Downscaling of GCM projections to finer spatial and temporal scales appropriate for hydrological modelling presents a third source of uncertainty.

The final source of uncertainty in climate change hydrological impact assessments is associated with the hydrological models used to translate climatological changes to hydrological impacts. Alternative hydrological models that produce acceptable results for an

observed baseline period may respond differently when forced with the same climate change scenario (Gosling and Arnell, 2011; Haddeland *et al*., 2011). Hydrological models include fully distributed, physically based models (e.g. Refsgaard *et al.*, 2010), which can detail a range of processes, potentially at a very fine spatial scale (e.g. Thompson *et al.*, 2004; Hammersmark *et al.*, 2008), but which require an extensive range of data. Semi-distributed or lumped models (e.g. Arnold *et al.*, 1998) adopt a more conceptual approach for process description, whilst global hydrological models (e.g. Döll, 2003; Gosling and Arnell, 2011) employ large model grid sizes and simplified process descriptions.

Investigation of uncertainty within climate change hydrological impact assessments has often focused on GCM uncertainty. Methods have included perturbed physics ensembles, in which perturbation of the parameterisations within a single or a series of GCMs are employed to provide many realizations of climate that can be used within hydrological modelling studies. The 2009 UK Climate Projections (UKCP09, Jenkins *et al.*, 2009), for example, are based on a large perturbed physics ensemble using the Met Office Hadley Centre's HadCM3 GCM and results from another twelve GCMs. Simple conceptual hydrological models of different wetland types have been driven with all the realizations from the UKCP09 projections to provide regionalized frequency distributions of the hydrological and, in turn, ecological impacts of climate change (Acreman *et al.*, 2012). Similarly, Prudhomme *et al.* (2003) used a Monte Carlo approach to define 25,000 climate scenarios for simulation of a number of UK catchments using a conceptual rainfall-runoff model. However, these approaches are computationally intensive, especially with complex hydrological models. A more common approach to investigating GCM uncertainty is to use a range of projections for the same emissions scenario derived from an ensemble of GCMs (e.g. Meehl *et al.*, 2007).

This approach was used within the UK Natural Environment Research Council QUEST-GSI (Global Scale Impacts) project (http://www.met.reading.ac.uk/research/quest-gsi/), in which hydrological models for catchments around the world were employed to assess the impacts of a consistent set of climate change scenarios. For each catchment, only one hydrological model was utilised, giving no indication of the impact of choice or structure of hydrological model upon climate change impacts. Prudhomme and Davies (2009) suggest that this is relatively common, with hydrological model uncertainty often being ignored within impact studies. Where different hydrological models of the same catchment exist, they have invariably been developed by different institutions and for different purposes, and are therefore rarely used to assess the same climate change scenarios. The impact of hydrological model-derived uncertainty on climate change impacts may not, however, be negligible (e.g. Dibike and Coulibaly, 2005; Haddeland *et al*., 2011; Hagemann *et al*., 2012). The QUEST-GSI project provided an initial assessment of some of these issues through a comparison of catchment hydrological model results with those of the Mac-PDM.09 global hydrological model (Gosling and Arnell, 2011) for the same GCM / global mean temperature change scenarios (Gosling *et al.*, 2011a). The comparison was, however, limited to the catchment outlet, whereas in some of the larger catchments, hydrological models provided distributed responses in river flow from major sub-catchments.

The current study builds upon this earlier work, with a particular focus on one of the QUEST-GSI catchments. The Mekong is one of the world's major rivers. It flows through a catchment with spatially variable climate, topography and land cover and supports a large and growing human population. Climate change may exacerbate the already significant changes resulting from development within the catchment. A model of the Mekong is created using MIKE SHE, a fully distributed hydrological modelling system combining both physically based and conceptual components (see below). As far as possible, this model employs the same data as

the model of the basin used within the QUEST-GSI project (Kingston *et al.*, 2011). A more robust calibration enables the investigation of the response to the QUEST-GSI climate change scenarios throughout the catchment. These results are subsequently compared to those that are available for the earlier catchment model as well as those from the Mac-PDM.09 global hydrological model.

2. Materials and methods

2.1. The Mekong Catchment

The Mekong is the largest river in southeast Asia. It is the world's eighth largest in terms of annual discharge (475 km^3), 12th longest (c. 4,350 km) and 21st largest by drainage area (795,000 km^2) (e.g. Kiem *et al.*, 2008). Rising in the Tibetan Highlands at an elevation of over 5,100 m, it passes through China, Burma, Laos, Thailand, Cambodia and Vietnam (Figure 1). Major tributaries include the Chi and Mun, which drain the Korat Plateau of eastern Thailand and join the Mekong upstream of Pakse, and the Se Kong and Sre Pok, which rise in Vietnam's Central Highlands and flow into the Mekong at Stung Treng. Further downstream, the river both provides water to and drains the Tonle Sap Lake, depending upon the season, before discharging into the South China Sea via the distributaries of the Mekong Delta.

In the upper catchment (the Lancang) the river and its tributaries flow through narrow, steep gorges. Land cover consists of tundra and montane semi-desert. Further downstream, below Chiang Saen, the river becomes largely navigable except for a few waterfalls. Natural vegetation is dominated by evergreen and deciduous forest (Ishidaira *et al.*, 2008). Rapid economic development and a growing population (currently 60 million and projected to

increase to 90 million by 2025 (MRC, 2003)) have driven the expansion of agriculture and consequent deforestation, leading to a large reduction in forest extent (Nobuhiro *et al.*, 2008).

The dominant climatic influence on the Mekong is the Asian monsoon. The rainy southwest monsoon begins in mid-May and extends into early-October. Over 90% of annual precipitation falls within this period (Kite, 2001). Annual precipitation ranges from under 1000 mm on the Korat Plateau to over 3200 mm in mountainous parts of Laos. In the upper parts of the basin within the Tibetan Highlands and Yunnan, precipitation falls both as rain and snow, the latter in particular during the relatively dry November–March period when snow covers approximately 5% of the total Mekong catchment (Kiem *et al.*, 2005). Snowmelt is responsible for the initial rise in the annual flood season within the Lancang sub-catchment. The Mekong River begins to rise in May and peak discharges are attained between August and October, after which they decline, reaching their lowest levels in March–April.

The Mekong has been identified as a hotspot of global change (Takeuchi, 2008). Rapid development and population growth have resulted in the previously discussed deforestation. Linked to these developments are increasing competition for water, contamination of water by agriculture, industry and settlements, and unsustainable use of resources such as fisheries, which currently sustain around 300 million people within and outside the catchment (MRC, 2003). Dams in upstream parts of the catchment, most notably the Manwan (constructed in 1993) and the Dachaoshan (2001), have been implicated in changes in flow regime, sediment flows and fisheries (Hapuarachchi *et al.,* 2008; Li and He, 2008; Kummu *et al.*, 2010; Wang *et al.*, 2011) and more are planned which will likely exacerbate these changes (Stone, 2010).

Whilst useful and informative modelling studies have been undertaken for the Mekong, some have only adopted future climate projections from a single GCM or ensemble means, thereby

not addressing climate model structural uncertainty (Kingston *et al.*, 2011). For example, Kiem *et al.* (2008) only used the Japanese Meteorological Agency GCM and the IPCC SRES A1b scenario within a gridded hydrological model of the catchment, whilst Ishidaira *et al.* (2008) employed the mean of the Tyndall Centre v2.03 scenario set within a distributed hydrological model. To address these issues, Kingston *et al.* (2011) used the model of the Mekong developed by Kite (2000, 2001) using the Semi-distributed Land Use-based Runoff Processes (SLURP, v.12.7) model (Kite, 1995). This model was used to assess the impacts of the consistent set of climate change scenarios used throughout the QUEST-GSI project (Todd *et al.*, 2011). The data employed within the SLURP model provided the starting point for the development of the MIKE SHE model of the Mekong.

2.2. MIKE SHE model development

MIKE SHE can be described as a deterministic, fully distributed and physically based hydrological modelling system (Graham and Butts, 2005). It is a comprehensive model for simulating the major processes of the land phase of the hydrological cycle and has been used in environments ranging from major international river basins (Andersen *et al.,* 2001; Stisen *et al.*, 2008), through catchments of hundreds or thousands of km^2 (Feyen *et al.*, 2000; Huang *et al.*, 2010; Singh *et al.*, 2010, 2011), to small (<50 km^2) catchments (Sahoo *et al.*, 2006; Dai *et al.*, 2010; Thompson, 2012). MIKE SHE has undergone decades of development from the original Système Hydrologique Europeén (Abbott *et al.*, 1986a,b). It now includes a range of process descriptions, some of which are more conceptual and semi-distributed in nature. These have advantages including a reduction in data requirements and reduced complexity compared to physically based solutions, and hence gains in execution time. An example is the linear reservoir saturated zone module which defines a series of sub-catchments, in turn divided into interflow and baseflow reservoirs based on topography, with exchanges between

reservoirs, and ultimately the MIKE 11 hydraulic model (Havnø *et al.*, 1995), being controlled by time constants. This method is particularly useful in large catchments (e.g. Andersen *et al.,* 2001; Stisen *et al.*, 2008) and so was employed within the model of the Mekong.

The 1 km × 1 km USGS GTOPO30 DEM employed by Kite (2000, 2001) for the SLURP Mekong model was used within the MIKE SHE model. The topographic grid was used to define the Mekong catchment boundary and 17 sub-catchments for the linear reservoir saturated zone module (Figure 1). Sub-catchments were established based on a combination of the location of the gauging stations for which data for model calibration / validation were available, the major tributaries of the Mekong and large changes in the topographic character (Figure 1). The sub-catchments included the Tonle Sap and the Mekong Delta which, following Kite (2001), was simplified to one channel. This, and the limited flow data available for the Tonle Sap River and the Delta, meant that the most downstream location for which model results were reviewed was Phnom Penh. For each sub-catchment, the same topographic data were used to define the extent of three interflow reservoirs such that each covered approximately one-third of the sub-catchment area (Figure 1). Two baseflow reservoirs were specified within each sub-catchment to represent the faster and slower baseflow storage, with their extent defined as the sub-catchment boundaries. The two time constants (interflow and percolation) for each interflow reservoir and the baseflow time constant for both baseflow reservoirs (i.e. eight for each sub-catchment), as well as the dead storage proportion for the lower baseflow reservoir, were varied during model calibration.

The distribution of soil classes within a two-layer water balance unsaturated zone module (Yan and Smith, 1994) was specified as a 1 km × 1 km grid based on the FAO Digital Soil Map of the World (FAO, 1990). Using the approach adopted by Andersen *et al.* (2001) and Stisen *et al.* (2008), soils were aggregated into four broad categories based on textural classes (Coarse

/ Medium, Medium, Medium / Fine and Fine). Infiltration rate and percentage water content at saturation, field capacity and wilting point for each soil category were taken from the literature (Clapp and Hornberger, 1978; Carsel and Parrish, 1988; Marshall *et al.*, 1996). Glaciers are an additional FAO class within the catchment. These are located in small areas in the Lancang and cover just under 0.9% of the total catchment. An infiltration rate of 0 m s^{-1} and a uniform 100% soil moisture water content were applied, although the small total area covered by this category meant that model results were insensitive to these parameter values.

Vegetation distribution was represented by the 1 km × 1 km land cover grid specified within the SLURP model and presented by Kite (2001). This was originally derived from the USGS Global Land Cover Characterization dataset, with the 24 land cover classes aggregated into nine categories (% of total catchment, dominant distribution within the catchment): agriculture and pastureland (38%, dominant in the Korat plateau and lower Mekong), evergreen forest (20%, concentrated in Vietnam's Central Highlands), mixed forest (13%, lower Lancang and sub-catchments above Vientiane), deciduous forest (9%, distributed in small patches with other forest types), grassland and semi-desert (10%, restricted to the upper and middle Lancang), shrubland (8%, dominant in lower sections on the Lancang), water (1.3%, concentrated in the Tonle Sap Lake), tundra (0.6%, wholly within the upper Lancang), and urban (0.1%, concentrated in major urban centres such as Phnom Penh and Vientiane). Variation in leaf area index through the year for each land cover, which is required in the MIKE SHE interception and evapotranspiration modules, was taken from Kite (2000) and based on a monthly time series of NDVI derived from NOAA AVHRR imagery. Root depths were taken from the literature (Kelliher *et al.*, 1993; Jackson *et al.*, 1996) and an existing DHI (2009) vegetation properties file.

The SLURP land cover grid, but with all forest types combined into one category, was used to spatially distribute Manning's M for overland flow resistance. Values were taken from the literature (Chow, 1959; Vieux, 2004; Sahoo *et al.*, 2006) and previous experience of MIKE SHE model development (Thompson *et al.*, 2004; Thompson, 2012), with a hierarchy from urban (least resistance and therefore highest Manning's M) to forest (greatest resistance).

The plan of the main river channels was digitised as a MIKE 11 river network (Figure 1) from that employed within the SLURP model (Kite, 2001). Cross-sections from Shopea (2003) and the Mekong River Commission (http://ffw.mrcmekong.org/) were used to establish representative maximum cross-section depths and cross-section profiles for different stream orders. Overlaying the channel network onto Google Earth Pro enabled channel widths and, when combined with the depth and cross-section profile for the relevant stream order, cross-sections to be specified throughout the model. Cross-sections were specified as depths relative to the bank, with the bank elevation taken from the relevant MIKE SHE topographic grid square (Thompson *et al.*, 2004). Manning's n values were taken from Chow (1959). Since many of the dams identified by Kite (2000) as constructed or planned within the catchment are not currently in place, were completed after the calibration period, or are relatively small with limited information on their operation, they were not represented within the model.

Meteorological inputs of precipitation, temperature and potential evapotranspiration (PET) were spatially distributed using the sub-catchments employed within the SLURP model (Figure 1). These were broadly similar to those specified within the MIKE SHE linear reservoir saturation zone module. However, the Lancang was defined as one sub-catchment in SLURP, whereas three separate linear reservoir sub-catchments were defined for this part of the Mekong within MIKE SHE. Similarly, the additional number of gauging stations used for model

calibration / validation (see below) resulted in the division of the central part of the Mekong into a series of linear reservoirs replacing the one large SLURP sub-catchment.

Since an aim of the current study is to compare results between the MIKE SHE model and those from Kingston *et al.* (2011), it was considered appropriate to maintain the original distribution of meteorological inputs. Monthly precipitation totals and mean temperature were obtained from the 0.5° resolution University of Delaware global precipitation dataset (UDel; Legates and Willmott, 1990) and the CRU TS 3.0 dataset (Mitchell and Jones, 2005), respectively. Monthly data from the 268 grid cells covering the Mekong catchment were then stochastically disaggregated to daily resolution following the procedures of Arnell (2003) as described by Todd *et al.* (2011). This required the coefficient of variation for precipitation and standard deviation for temperature from station-based data provided by the US National Climate Data Centre (NCDC) global surface summary of the day (GSOD) meteorological stations previously employed by Kite (2001). Mean daily precipitation and temperature were subsequently evaluated for each sub-catchment used to distribute meteorological inputs.

Precipitation lapse rates for those sub-catchments with a large range in elevation were modified during model calibration. Similarly, a temperature lapse rate was included over the Lancang, the one sub-catchment in which snow cover is a regular feature. This lapse rate was adjusted so that the range of temperatures and number of months when temperature was below 0 °C within specific MIKE SHE grid squares approximated those at GSOD meteorological stations located within these grid squares. Monthly PET was evaluated for each of the sub-catchments employed to distribute meteorological data using the Linacre method, the same PET scheme employed by Kingston *et al.* (2011). Monthly totals were distributed evenly throughout the month, following initial experiments that showed model results to be insensitive to this method compared to the application of daily estimates of PET.

Although all gridded data were specified using a 1 km × 1 km grid, the computational grid employed by the model was increased in size to 10 km × 10 km following a series of experimental runs which showed little change in simulated river discharge for grid sizes between 1 km and 20 km (see Vásquez *et al.*, 2002; Thompson, 2012). The larger grid size resulted in logistically appropriate computation times for the application of the autocalibration routines discussed below. This balance between computation time and representation of catchment attributes is common with distributed hydrological models (McMichael *et al.*, 2006). Within MIKE SHE, all input data were automatically resampled to the larger grid. Hypsometric curves derived from the resampled and original topography are very similar, as are the relative importance of the different soil and land use categories, suggesting that the larger grid retains a good representation of catchment characteristics.

2.3. Model calibration and validation

In common with Kingston *et al.* (2011), a baseline period of 1961–1990 was used for calibration and the shorter 1991–1998 period for validation. Whereas SLURP was only calibrated using three stations (Chiang Saen, Pakse and Ubon, Figure 1), data from a further nine gauging stations were used for MIKE SHE (Figure 1). Eight of these are on the main Mekong and the other (Yasothon) on a tributary, the Chi. Although daily discharge data were available for the full calibration period for the majority of these stations, the records for Stung Treng, Kompong Cham and Phnom Penh were limited to January 1961–December 1969, January 1964–March 1974 and January 1961–March 1974, respectively. The discharge data for Kratie, which were available for the 30 year calibration period, were derived by Kite (2000) using Pakse discharge and methods developed by the Institute of Hydrology (1988).

Calibration was undertaken using the time constants of the saturated zone linear reservoirs, the dead storage proportion for the lower baseflow reservoirs, and, in sub-catchments with a wide elevation range, precipitation lapse rate. The snowmelt degree-day coefficient was varied during calibration of the Lancang at Chiang Saen, this being the one sub-catchment with snow cover. Following calibration, a review of the simulated snow cover was undertaken to confirm that extensive snow was only present during the period November–March and that its maximum extent was approximately equivalent to 5% of the total catchment area (e.g. Kiem *et al.*, 2005). Calibration was undertaken for each gauging station in a downstream sequence beginning at Chiang Saen and progressing to Mukdahan. The Chi and Mun sub-catchments (Yasothon and Ubon gauging stations) were then calibrated before continuing the calibration for the gauging stations between Pakse and Phnom Penh. In each case, only those model parameters for sub-catchments between the previously calibrated upstream gauging station and the current station were varied.

Initially, an automatic multiple objective calibration was undertaken based on the shuffled complex evolution method (Duan *et al.*, 1992; Madsen, 2000, 2003). Two equally weighted calibration criteria, the absolute value of the average error and the root mean square error, were employed (Butts *et al.*, 2004), and these were aggregated into one measure using a transformation that compensates for differences in the magnitudes of the criteria (Madsen, 2003). The autocalibration routine evaluated the two calibration criteria at the model time step (defined as a maximum of 48 hours). However, as acknowledged by Kingston *et al.* (2011), there is a disconnect between the daily meteorological input data and discharge as a result of generating the daily meteorological data using a stochastic weather generator.

Whilst model performance following autocalibration was generally good, it was possible to improve it through manual modification of model parameters, with observed and simulated

discharge being aggregated to mean monthly flow (Kingston *et al.*, 2011). Model performance at each gauging station was assessed using the Nash-Sutcliffe coefficient (NSE, Nash and Sutcliffe, 1970), the Pearson correlation coefficient (r) and the percentage deviation in simulated mean flow from the observed mean flow (Dv; Henriksen *et al.*, 2003). The scheme of Henriksen *et al.* (2008) was used to classify the model performance as indicated by NSE and Dv.

Following calibration, the implications of using the stochastic weather generator to disaggregate monthly precipitation and temperature to a daily time step was investigated using eight different outputs from the weather generator for both meteorological inputs. All possible combinations of these time series were employed (i.e. 64 runs). Calibration statistics were evaluated for each run. Subsequently, the model was run for the shorter 1991–1998 period for validation. Data for two of the gauging stations used for calibration, Kompong Cham and Phnom Penh, were not available for this period, whilst the length of records for the remaining ten stations varied from the complete eight years to only three years.

2.4. Simulation of climate change

The same revised meteorological inputs as used by Kingston *et al.* (2011) were employed to simulate potential impacts of, and uncertainty associated with, climate change. Future (monthly resolution) climate scenarios for temperature and precipitation were derived using the ClimGen pattern-scaling technique (Arnell and Osborn, 2006) for a 30 year period. ClimGen, a spatial scenario generator, employs the assumption that the spatial pattern of climate change, expressed as change per unit of global mean temperature, is constant for a given GCM. In this way, it is possible for the pattern of climate change from a GCM to be scaled up and down in magnitude. This enables the impacts of specific thresholds of global climate

change to be investigated (Todd *et al.*, 2011). Scenarios were generated for a prescribed warming of 2 °C, the hypothesised threshold for 'dangerous' climate change (Todd *et al.*, 2011), for seven GCMs: CCCMA CGCM31, CSIRO Mk30, IPSL CM4, MPI ECHAM5, NCAR CCSM30, UKMO HadGEM1 and UKMO HadCM3. These were selected from the CMIP-3 database (Meehl *et al.*, 2007) as exemplar GCMs representing different future representations of global climate system features. In addition, the UKMO HadCM3, a widely employed GCM previously used for model uncertainty analysis (e.g. Murphy *et al.*, 2004), was selected to derive scenarios for prescribed warming of global mean temperature of 1, 2, 3, 4, 5, and 6 °C.

Monthly scenario Linacre PET was calculated for each GCM grid square and, as for baseline meteorological data, distributed on a daily basis evenly throughout each month. Scenario precipitation and temperature for each GCM grid square were downscaled to daily resolution using the stochastic weather generator. Precipitation, temperature and PET were averaged for each meteorological sub-catchment. Separation of the river discharge climate change signal into that attributable to modifications in precipitation, PET and temperature was investigated by in turn specifying scenario time series for one of the three meteorological inputs whilst employing baseline time series for the other two (Kingston *et al.,* 2011; Thompson, 2012). This was undertaken for both sets of climate change scenarios.

2.5. Inter-hydrological model comparison

As discussed above, a less frequently considered source of uncertainty in climate change hydrological impact assessments is hydrological model uncertainty (Prudhomme and Davies, 2009). In this study, an assessment of such uncertainty was undertaken using results from three alternative hydrological models for the same two sets of climate change scenarios. Table 1 summarises the key attributes of these three hydrological models, including the type of

model, the meteorological inputs employed and the spatial distribution of meteorological inputs, catchment characteristics and process simulation.

The first hydrological model is the MIKE SHE model developed in the current study that comprises a combination of spatially distributed, physically based and semi-distributed, conceptual process descriptions. The SLURP model of the Mekong developed by Kite (2000, 2001) and refined by Kingston *et al.* (2011) provides the second hydrological model. SLURP is a semi-distributed, conceptual model that uses a combination of sub-basins and land cover classifications to define model elements in an approach similar to the hydrological response units used within models such as SWAT (e.g. Arnold *et al.*, 1998). Vertical water balances are subsequently evaluated for each of these elements, with results being aggregated at the sub-catchment scale. Of the 12 gauging stations used in the current study to present MIKE SHE results (Figure 1), results from SLURP for the same climate change scenarios were available for three stations: Chiang Saen, Pakse and Ubon (although results for the latter station were not presented in the earlier study).

The third hydrological model is Mac-PDM.09 ("Mac" for "macro-scale" and "PDM" for "probability distributed moisture model"), an established global hydrological model that simulates runoff across the global land surface domain (Arnell, 1999b; Arnell, 2003; Gosling and Arnell, 2011). It calculates the daily water balance in each of the 67,420 0.5° × 0.5° cells across the global land surface, treating each cell as an independent catchment. Runoff is generated from precipitation falling on the portion of a cell that is saturated, and by drainage from water stored in the soil. Mac-PDM.09 was not specifically calibrated for the Mekong; instead, the model was calibrated at the continental scale by 'tuning' it to help define parameter values. This involved tests of precipitation datasets and potential evaporation calculations and comparisons with long-term average runoff and within-year runoff patterns

for a small number of major river basins and for a large number of small basins (see Arnell, 1999b). The performance of Mac-PDM.09 was recently evaluated by validating simulated runoff against observed runoff for 50 catchments across the globe, and the model was found to perform well (Gosling and Arnell, 2011). Moreover, a recent inter-hydrological model comparison exercise showed that Mac-PDM.09 performed as well as other global hydrological models in terms of simulating the patterns and magnitudes of observed global runoff (Haddeland *et al.*, 2011).

For comparison with results from MIKE SHE and SLURP, simulated runoff from Mac-PDM.09 for each climate change scenario was aggregated at a monthly time step for all the model grid cells within the boundaries of the catchments of six gauging stations: Chiang Saen, Vientiane, Nakhon Phanom, Pakse, Phnom Penh and Ubon (Figure 1). These were selected in order to provide a comparison of results for the three gauging stations for which results are available for all three hydrological models (Chiang Saen, Pakse and Ubon). Vientiane and Nakhon Phanom were selected as stations in the middle of the catchment upstream of the two major tributaries draining the Korat Plateau (the Chi and Mun), whilst Phnom Penh is the lowest station on the river and upstream of the ecologically and economically important Mekong Delta. Comparisons of results for these stations are limited to MIKE SHE and Mac-PDM.09. This analysis extends the preliminary inter-model comparison undertaken by Gosling *et al.* (2011a) that was limited to a comparison of SLURP and Mac-PDM.09 for Pakse alone.

3. Results

3.1. Model calibration and validation

Model performance statistics derived for the 1961–1990 period for the 12 gauging stations used in model calibration are provided in Table 2. As indicated above, these are derived from mean monthly discharges. For Stung Treng, Kompong Cham and Phnom Penh, statistics are based upon the reduced periods of observed discharge. In the case of Chiang Saen, Pakse and Ubon, the values of Dv and NSE reported by Kingston *et al.* (2011) from the calibrated SLURP model of the Mekong are also provided. According to the classification scheme of Henriksen *et al.* (2008), the performance of the MIKE SHE model, as indicated by the values of Dv and NSE, can in general be classed as "excellent" (20 out of the 24 model performance statistics). Although an equivalent classification for the correlation coefficient is not employed, the value of this statistic is above or very close to 0.95 for ten of the 12 gauging stations.

Figure 2 shows monthly mean observed and simulated discharge for five gauging stations along the main Mekong for the calibration period. These stations are selected as representative of results for the main stem of the Mekong above Kratie, the latter being the lowest gauging station for which flow data (albeit in this case derived from another station) are available for the full simulation period. Flow duration curves derived from observed and simulated mean monthly discharges at all gauging stations (not shown) confirm the good performance of the MIKE SHE model. When compared to SLURP, model performance at Chiang Saen is superior, with MIKE SHE Dv and NSE values exceeding those obtained using the earlier model (Table 2). Dv for SLURP falls in the "very good" as opposed to "excellent" category. Figure 3, which shows observed and simulated river regimes for all 12 gauging stations including those from SLURP for the stations where they are available, demonstrates a considerable overestimation by SLURP in recession discharge following the annual peak at Chiang Saen. In contrast, discharges at this time of year simulated by MIKE SHE more closely follow the observed. Similarly good reproduction of the river regimes at other stations between Chiang Saen and Pakse by MIKE SHE is also demonstrated. At the latter station, the

performance statistics are comparable for MIKE SHE and SLURP. A higher NSE value is obtained for the former, whilst simulated mean flow is closer to the observed for SLURP. However, Figure 3 demonstrates that the seasonal peak discharge (August) is underestimated by SLURP by on average nearly 2640 m^3s^{-1} (10%) compared to under 300 m^3s^{-1} (1.1%) for MIKE SHE (although in September underestimation by MIKE SHE increases to 4.6%).

Further downstream on the main Mekong, the values of Dv for Kompong Cham and Phnom Penh, for which discharge data is limited to the first half of the calibration period, fall below the "excellent" category and are instead classified as "very good" and "fair", respectively (Table 2). The NSE values for these two stations are still, however, classified as "excellent". Reduction in model performance at these two stations is evident in Figure 3, as simulated discharge leads observed more than at the other stations on the main Mekong for which data are available for the full calibration period. This feature is also evident (although to a smaller extent) at Stung Treng, where observed data are also limited in duration, suggesting that model performance may be influenced by this reduction in the length of observed discharge.

Model performance is relatively weak for the Chi and Mun sub-catchments (Table 2), with peak seasonal discharge being underestimated (Figure 3). In comparison to other gauging stations, simulated flows deviate further from the observed. During calibration it was not possible to raise peak discharges without increasing discharge during the annual rise and recession, which are reasonably well reproduced. These changes would result in overestimation of mean discharge causing Dv, currently classified as "excellent", to increase. This trade-off is evident in SLURP results for Ubon. Whilst the magnitude of the simulated peak corresponds well with the observed (Figure 3), overestimation of discharge through most of the rest of the year causes Dv to be classified as "very poor" (Table 2). The NSE value for this gauging station for MIKE SHE is a class above that of SLURP ("fair" compared to

"poor"). At Yasothon, the NSE value just falls short of the "fair" category. Therefore, although MIKE SHE does not perform as well for these two sub-catchments as it does for gauging stations on the main Mekong, results are considered to be superior to those of SLURP.

Results from the 64 runs over the same 30 year calibration period using the calibrated model and eight alternative precipitation and temperature time series from the stochastic weather generator showed that the model was not sensitive to the disaggregation procedure. NSE and r for Chiang Saen varied by only 0.03 and 0.02, respectively, whilst at Pakse the corresponding ranges were 0.02 and 0.01. Further downstream at Kratie, the ranges of both statistics were only 0.01. Very similar results were obtained for the other gauging stations. These findings concur with the results of Kingston *et al.* (2011), who employed a smaller set of 10 alternative model runs to assess the sensitivity of the SLURP model to weather generator inputs.

Table 3 shows performance statistics for the shorter validation period (1991–1998). As indicated, the length of observed discharge records varies between gauging stations. The corresponding values for Chiang Saen and Pakse reported by Kingston *et al.* (2011) are also provided (values for Ubon were not reported in the earlier study). Good performance of the MIKE SHE model is indicated, although performance is inferior to the calibration period. Where NSE values are available for SLURP, they are lower than those from MIKE SHE. Three NSE values retain the "excellent" classification whilst five are classified as "very good". The remaining two are classed as "fair". One of these (Stung Treng) is based on only three years due to limited observed data, whilst the other (Yasothon with five years of data) is the station with the largest underestimation of mean discharge. Values of r follow the pattern of NSE, with values above or close to 0.9 associated with "excellent" NSE values. Most values exceed 0.8, whilst those for Stung Treng and Yasothon are lower. Eight gauging stations have values of Dv that are classified as "very good", whilst Stung Treng and Yasothon are again classified

as “fair”. At all the gauging stations, mean discharge is, however, underestimated. SLURP results show that at Chiang Saen, overestimation of mean discharge for the calibration period is reduced for the validation period, whilst at Pakse, the slight overestimation of the calibration period is replaced by a larger underestimation for the later period.

In light of the relatively short validation period and given an emphasis of the current study to compare alternative models of the catchment using the same input data, the overall performance of the MIKE SHE model is considered appropriate. For the three (two) gauging stations for which results are available for SLURP for the calibration (validation) period, MIKE SHE results are generally superior. Similarly, MIKE SHE compares very favourably with previous models of the catchment, although precise comparisons are hindered by alternative performance statistics and simulation periods. For example, values of NSE for a number of gauging stations used by Hapuarachchi *et al.* (2008) varied between 0.7 and 0.83, predominantly lower than those obtained using MIKE SHE, with the exception of Yasothon and Ubon, whilst the model of Västilä *et al.* (2010) obtained an NSE for Kratie of 0.63 compared to 0.90 for the calibration period (validation: 0.73) in the current study.

3.2. Climate change scenarios: 2°C increase using seven GCMs

3.2.1. Changes in climate

Baseline annual precipitation and PET, and percentage changes from these totals, for each of the 2 °C, seven GCM scenarios are shown for eight sub-catchments in Table 4 (top half). Results for the other sub-catchments are not shown as they are relatively small and changes are represented by one or more of those in Table 4. Mean monthly precipitation and PET for the baseline and each scenario are shown for four sub-catchments in Figure 4. Again, these

are representative of changes over the remaining sub-catchments. Changes in temperature are not presented here since, in most sub-catchments, changes in temperature are reflected in modified PET. The exception is the Lancang, the one sub-catchment in which snow and its seasonal melt influences runoff. Changes in mean annual temperature over this sub-catchment range from +2.3 °C (CCCMA) to +2.9 °C (IPSL). Temperatures increase throughout the year in all scenarios with the largest changes (up to +3 °C) between October and March. Summer temperature increases are on average lower (+2.0–2.3 °C).

Wide variation in the magnitude and direction of annual changes in precipitation occurs between GCMs. These were described by Kingston *et al.* (2011) and are summarised here and in Table 4. CCCMA, MPI and NCAR exhibit increasing annual precipitation for all sub-catchments. Increases are greater in upstream sub-catchments for CCCMA and NCAR, and in downstream sub-catchments for MPI. CSIRO simulates reduced annual precipitation across all sub-catchments, whilst reductions occur across all but three south-central sub-catchments (Chi-Mun, Mekong 2 and Sre Pok) for IPSL. HadCM3 shows increased precipitation over the four most northern sub-catchments (Lancang to Mekong 1). Increases in this part of the catchment are restricted to the top two sub-catchments for HadGEM1, whilst precipitation also increases over the lower three sub-catchments.

Seasonal changes in precipitation also vary widely between GCMs (Kingston *et al.* 2011; Figure 4). CCCMA and NCAR experience peak increases in April and September, with decreases concentrated in November–February/March. A notable exception is Lancang for the CCCMA GCM, which experiences increasing precipitation in every month. Inter-seasonal changes in precipitation for the MPI GCM are, in contrast, unimodal, with increases being concentrated between May and November. For CSIRO, increases in precipitation are limited to September over upstream sub-catchments (e.g. Lancang and Mekong 1, Figure 4). This period

expands to June–September in the far south (e.g. Mekong 3). The distribution of change through the year for IPSL is also unimodal, with increases being limited to August–September and, in the far south, September–October (Figure 4). HadCM3 and HadGEM1 exhibit a bimodal distribution in the seasonal pattern of changes in precipitation, with the largest increases occurring in May and September (HadCM3) / October–November (HadGEM1).

Differences in the PET climate change signals between the seven GCMs are smaller than those for precipitation (Table 4, Figure 4). Annual PET increases across the Mekong for all GCMs. With the exception of three sub-catchments (Chi, Mun and Chi-Mun), the smallest increases in annual PET are associated with NCAR (on average +10.9%). In the three sub-catchments where this is not the case, the lowest PET increases result from HadGEM1, although these are only slightly lower than those of NCAR. There is a systematic geographical pattern for the GCMs that produce the largest increases in annual PET. In the four most northerly sub-catchments (1–4, Figure 1), IPSL produces the largest changes (mean: +16.0%). In the middle Mekong (sub-catchments 5–9), the largest changes are associated with CSIRO (mean: +15.7%), followed by IPSL or HadCM3, whilst in the lower part of the catchment (sub-catchments 10–13), HadCM3 (CSIRO for sub-catchment 9) produces the largest increase in PET (mean: +15.5%), followed by CSIRO. Many of the GCMs show a relatively constant climate change signal throughout the year (Figure 4). Notable exceptions are the peaks for CSIRO in April and May and for MPI in April, which are most clearly evident in central and lower sub-catchments (e.g. Mekong 1, Mun and Mekong 3; Figure 4).

3.2.2. Changes in river flow

Table 5 presents the values of the mean, Q5 and Q95 (discharges exceeded 5% and 95% of the time, respectively) discharges for the baseline and the percentage changes in these discharges

for each of the 2 °C, seven GCM scenarios. These are provided for eight gauging stations which are representative of changes at the other four stations used in model calibration / validation. Mukdahan represents the changes at Nakhon Phanom approximately 100 km upstream. Similarly, discharge at Stung Treng, which is not shown, responds in the same way to Kratie (c. 150 km further downstream), whilst Phnom Penh is representative of the changes in simulated discharge at Kompong Cham (c. 90 km upstream). Results for the Mun at Ubon represent those in the smaller catchment of the Chi at Yasothon. The simulated baseline and scenario river regimes for the same eight gauging stations are shown in Figure 5.

Of the three GCMs for which precipitation increases in all sub-catchments, two (CCCMA and NCAR) result in increases in mean discharge for all gauging stations (Table 5). The magnitude of the changes is relatively uniform along the main stem of the Mekong for CCCMA, albeit with a small increase at stations in middle reaches (Mukdahan and Pakse). The much larger increase in mean discharge of the Mun at Ubon is indicative of other sub-catchments in this part of the catchment, which results in enhanced flows from these tributaries to the Mekong, although absolute magnitudes are relatively small. In the upper catchment (Chiang Saen), increasing annual discharge is a result of higher flows during the initial rise in discharge, which could be partially attributable to enhanced snowmelt, and then higher discharge during the recession and low flow period (Figure 5). Peak annual discharge is, however, slightly (<1%) lower and still occurs in August. As a result, Q5 decreases slightly, whilst Q95 increases (Table 5). Further downstream, peak flows begin to increase and by Vientiane, mean discharge in August and September are approximately equal. For gauging stations below Vientiane, discharges are higher in September than August, the opposite for baseline river regimes. This is due to the large September increases in precipitation.

A similar pattern of change occurs for NCAR, although in most cases changes are larger than those associated with CCCMA (particularly in the middle section of the catchment between Luang Prabang and Pakse; Table 5). Table 4 shows that whilst increases in precipitation over this part of the catchment are smaller for NCAR compared to CCCMA, PET rises by smaller amounts for NCAR, accounting for the enhanced river flow. A relatively consistent change in the river regime at all stations is shown in Figure 5. Baseflows are higher, especially in the upstream part of the catchment, and the seasonal rise begins slightly earlier, although for the majority of this period, deviations from the baseline are small. The month of highest mean discharge shifts from August to September, although (with the exception of Chiang Saen) mean discharge in August also increases. Following the peak, discharges during the recession are higher than the baseline, especially in upper and middle parts of the catchment.

Precipitation increases in all sub-catchments for MPI. However, the magnitude of these changes is relatively small in upstream parts of the catchment compared to CCCMA and NCAR, whilst increases in PET are larger than for these two GCMs (Table 4). Mean annual flow at Chiang Saen and Luang Prabang therefore decline (by 2.3% and 1%, respectively, Table 5). Below these stations, gains in precipitation are larger and mean discharge increases in a downstream direction, although by smaller amounts than for CCCMA and NCAR (Figure 5). Where mean discharge declines it is largely due to reductions in the post-peak recession. Flows at other times only increase by very small amounts. As a result, Q5 increases, whilst Q95 experiences very modest declines at most gauging stations except for Pakse (small increase) and Ubon (a larger increase of 6.8%).

The patterns of change in mean, Q5 and Q95 discharge for the CSIRO and IPSL GCMs are broadly similar (Table 5). All three discharge measures decline at stations on the Mekong (Q5 increases at Ubon for IPSL) for both GCMs, with CSIRO resulting in consistently larger

reductions. The magnitude of reductions in mean flow and Q95 reduce in a downstream direction for both GCMs and for Q5 in the case of CSIRO. There are some departures from this trend in Q5 for ISPL, with relatively small reductions at Pakse due to increased wet season and mean annual precipitation in this part of the catchment. The river regimes from both GCMs display a delayed response in the annual rise in river discharge, whilst discharge during the post-peak recession and the dry season are relatively unaffected (Figure 5). On average, mean discharge for each month declines at stations on the Mekong for CSIRO and there is a shift from August to September for peak flows. On the Mun at Ubon peak discharge, which occurs in October, exceeds the baseline. Results for ISPL show a gradual downstream shift from peak flows occurring in August (Chiang Saen and Luang Prabang), through approximately equal mean discharge in August and September (Vientiane), to September discharge exceeding flows in August (Nakhom Phanom and downstream). On the Mun and Chi tributaries, mean discharges in September and October exceed those of the baseline.

Increases in annual precipitation for the Lancang and Nam Ou for HadGEM1 result in a small (<0.5%) increase in mean annual discharge at Chiang Saen. Further downstream, discharge declines, with the magnitude of reductions increasing with movement downstream until Pakse (Table 5). Modest increases in annual precipitation over the lower catchment stops this trend, with reductions in mean discharge for the stations between Stung Treng and Phnom Penh ranging between 9.0% and 9.1%. Q5 and Q95 discharges respond in a similar way. The largest changes in river regimes are reductions in discharge concentrated in August and September, the period of peak flow (Figure 5). Between Stung Treng and Phnom Penh, mean discharge in these months declines by on average 17.9% and 13.7%, respectively.

The large increases in annual precipitation over the Lancang and their extension further downstream for HadCM3 ensures that mean discharge increases between Chiang Saen and

Pakse, albeit with a downstream reduction in magnitude (Table 5). Further downstream, in response to declining precipitation and higher PET, mean discharges decline. Throughout the catchment, August remains the month of peak discharge, although mean discharge in this month declines (Figure 5). Increases in mean discharge in the upper catchment are largely driven by higher discharge in September and the subsequent recession that also increases Q5 as far downstream as Vientiane. From Mukdahan downstream, mean discharges in both August and September are below the baseline (by 6.7% and 4.7%, respectively at Phnom Penh). Very modest increases in dry season discharge are common to all gauging stations on the main Mekong and results in higher Q95 discharges (Q95 declines for Ubon).

Figure 6 summarises the percentage change in mean annual discharge at four representative gauging stations for each of the 2 °C, seven GCM scenarios. For each scenario, the corresponding changes resulting from the alternate specification of scenario time series for one meteorological input (precipitation, PET and temperature), whilst using baseline time series for the other two, are also shown. It is apparent that the inter-GCM differences are largely driven by differences in precipitation. As a result of the consistent increases in annual PET for the seven GCMs, mean discharge at all 12 stations declines if only scenario PET is specified. These declines occur in each month and the range of change in mean discharge at individual gauging stations is narrow (between a range of -3.6% for Phnom Penh and -6.3% for Yasothon), reflecting the relatively small inter-GCM differences in PET. In contrast, the much larger differences in precipitation between the GCMs ensure that the specification of scenario precipitation with baseline PET and temperature enhances the inter-GCM differences in discharge. The smallest range of change in mean discharge for gauging stations on the main Mekong (21.1%, between -3.2% and 17.9%) is for Phnom Penh compared to the largest (32.5%, between -6.8% and 25.7%) for Chiang Saen. Inter-GCM differences are larger on the two tributaries (e.g. 42.1%, between -10.0% and 32.1% for the Mun at Ubon).

Figure 6 demonstrates very small changes from the baseline when scenario temperature is employed with baseline precipitation and PET. Within the MIKE SHE model, changes in temperature are already incorporated within the alternative scenario PET, so that temperature influences snowmelt alone. As a result, the largest (but still small) changes in mean flow occur at Chiang Saen (reductions in mean discharge of between 0.04% and 1.2%), closest to parts of the catchment that experience snow cover. The magnitude of these changes declines downstream, and for tributaries in which snow is not a feature, changes in temperature alone have no impact on discharge (e.g. the Mun, Figure 6). Small changes in the river regime at Chiang Saen are associated with a slightly earlier increase in discharge due to earlier snowmelt and lower peak discharges, but variability between the different GCMs is small. For example, the increase in May discharge ranges from 19.9% to 25.0% (although absolute discharge is small), whilst August discharge declines by between 4.4% and 5.4%.

3.2.3. Comparison of MIKE SHE results with SLURP and Mac-PDM.09

Figure 7 shows percentage changes in mean discharge (runoff for Mac-PDM.09) at six gauging stations for each of the 2 °C, seven GCM scenarios, as simulated by the three hydrological models. As described above, results are only available for three stations for SLURP. Direction of change in mean discharge (runoff) for a given GCM is predominantly the same for all the hydrological models. Of the 42 gauging station / GCM combinations (six stations / seven GCMs), only three exhibit changes in mean discharge (runoff) which differ in sign between hydrological models. These are for stations towards the southern part of the catchment. Results for HadCM3 for Pakse show increases in discharge (runoff) for MIKE SHE and Mac-PDM.09. For MIKE SHE, the climate change signal (mean discharge: +1.4%) is the smallest of all the GCMs at this station, and SLURP shows a reduction in mean discharge of a comparable

magnitude (-1.6%). In contrast, Mac-PDM.09 runoff increases by 8.4%. At Phnom Penh, this same GCM is associated with a reduction in MIKE SHE mean discharge of 2.1%, whilst Mac-PDM.09 runoff increases by 2.5% (SLURP results are not available). Finally, at Ubon, both MIKE SHE and SLURP simulate reductions in mean discharge (of 3.0% and 5.1%, respectively) for the IPSL GCM, whilst mean runoff from Mac-PDM.09 increases by a very small amount (0.5%). Beyond these differences there is general agreement in the order of magnitude of changes for the seven GCMs for the different hydrological models. At most stations, when listed in order of increasing change in mean discharge, the GCMs appear in the same order for both MIKE SHE and Mac-PDM.09, with the exception, in most cases, of a single pair of GCMs.

Where mean discharge (runoff) at a gauging station increases for an individual GCM for all three hydrological models (MIKE SHE and Mac-PDM.09 where SLURP results are not available), the smallest changes are for SLURP, followed by MIKE SHE and then Mac-PDM.09 (Figure 7). The greater increases for Mac-PDM.09 are particularly apparent at upstream stations. At Chiang Saen, the percentage increase in mean runoff for Mac-PDM.09 for the four GCMs associated with increased mean river flow is on average 5.7 and 3.8 times as large as those of SLURP and MIKE SHE, respectively. These values are skewed by large changes for HadCM3 and large inter-hydrological model differences (but small absolute changes) for HadGEM1. HadCM3 stands out as a GCM for which differences between the catchment and global hydrological models are particularly large, especially in upstream parts of the Mekong. Percentage increases in mean runoff at Chiang Saen for Mac-PDM.09 for HadCM3 are 9.4 and 4.1 times as great as those for SLURP and MIKE SHE, respectively. Further downstream, inter-hydrological model differences in the magnitude of increases in discharge / runoff (when they occur for all the models) are smaller. This is exemplified in results for Ubon, where the increases in runoff for Mac-PDM.09 for the three GCMs with higher river flow for three

hydrological models are, on average, less than 1.4 times as large as the increases in MIKE SHE discharge. Mac-PDM.09 increases are still 4.6 times as large as those simulated by SLURP.

The dominant trend for GCMs associated with declines in annual flow at gauging stations on the main Mekong for all (both) hydrological models is for the largest changes to result for Mac-PDM.09, followed by MIKE SHE and SLURP (Figure 7). Exceptions are MPI at Chiang Saen and CSIRO at Pakse, where the reverse order of magnitude of changes occurs whilst, as noted above, at Phnom Penh MIKE SHE simulates a decline in mean discharge for HadCM3 whilst mean runoff increases for Mac-PDM.09. Inter-model differences (in particular between MIKE SHE and Mac-PDM.09 and especially downstream of Chiang Saen) in the magnitude of the declines are smaller than for those GCMs where river flow increases. For three GCMs, reductions in the mean discharge at Ubon are larger for MIKE SHE than for Mac-PDM.09 (and, as discussed above, for IPSL MIKE SHE mean discharge declines whilst mean runoff for Mac-PDM.09 increases slightly). Results for SLURP for Ubon show that, in most cases, reductions in mean discharge are larger (when they occur) than for the other two models. Differences between MIKE SHE and SLURP are relatively small. The exception is HadGEM1, where the decline in SLURP discharge is of a similar magnitude to that of Mac-PDM.09.

Following the approach of Gosling *et al.* (2011a), Figure 8 shows mean monthly total discharge (runoff for Mac-PDM.09) expressed as a percentage of the annual total for five (three in the case of SLURP) gauging stations simulated by the three hydrological models for the baseline and each of the 2 °C, seven GCM scenarios. Results for Vientiane, which are not shown in the interests of clarity, are similar to those for Nakhon Phanom. Given the dominant seasonal precipitation signal of the Asian monsoon, it is unsurprising that all three hydrological models simulate large seasonality in river flow. The amplitude of this cycle is, however, greater for Mac-PDM.09. Beyond this, the most obvious differences in the seasonal

cycle simulated by the three hydrological models are associated with the scenario results for Chiang Saen. SLURP simulates a consistent earlier rise in the annual hydrograph, which Kingston *et al.* (2011) attributed to earlier snowmelt and a subsequent smaller proportion of the annual total discharge occurring in peak months for all the scenarios. This is not the case for MIKE SHE or Mac-PDM.09. MIKE SHE simulates some modest increases in early season (May) discharge for some scenarios, but both this model and Mac-PDM.09 simulate a reduced significance of flows during subsequent months (June and July) for the same scenarios. The greater concentration of annual flows in August and September for some scenarios is evident for MIKE SHE and Mac-PDM.09. The increased significance of flows in the first of these months for IPSL is clearly evident, although the significance of September flows also increases for CSIRO and NCAR. This consistency between MIKE SHE and Mac-PDM.09 is repeated for Nakon Phanom.

The broad agreement between MIKE SHE and Mac-PDM.09 is repeated for the other two gauging stations further downstream on the main Mekong. Figure 8 shows that for Pakse the influence of the earlier rise in discharge simulated by SLURP has diminished, although scenario results still suggest greater significance of discharge at this time of year for many for the GCMs, which is contrary to MIKE SHE and Mac-PDM.09 (with the exception of MPI). MIKE SHE does show some consistency with the results of the other two models, such as the shift of peak flows from August to September for GCMs including CSIRO, IPSL and NCAR. Results for Ubon show a general agreement between the three hydrological models. Both MIKE SHE and SLURP simulate a greater concentration of the annual total discharge in October for all the GCMs with the exception of HadGEM1 for SLURP (an almost negligible decline). Mac-PDM.09 simulates similar increases for five GCMs although for CCCMA and MPI runoff in this month decreases slightly in significance. Other inter-model similarities include the increase in the significance of discharge during the latter part of the annual rise (August) for the MPI GCM.

3.3. Climate change scenarios: 1–6°C increase using HadCM3

3.3.1. Changes in climate

Table 4 (lower half) presents mean annual precipitation and PET for eight representative meteorological input sub-catchments for each of the 1–6 °C, HadCM3 scenarios. Mean monthly precipitation and PET for the baseline and each scenario are shown for four sub-catchments in Figure 9. Temperature changes are not presented and the patterns of these changes are reflected in the modifications to PET. Over the Lancang (where snow is a feature) changes in mean annual temperatures are above the prescribed increase in global mean temperature (for example 1.3 °C, 5.1 °C and 7.7 °C for 1 °C, 4 °C and 6 °C, respectively). In common with the 2 °C, seven GCM scenarios, largest temperature increases occur between October and March.

Changes in annual precipitation exhibit a distinct geographical pattern. Over the four sub-catchments that are furthest upstream (sub-catchments 1–4, Figure 1), annual precipitation increases in a consistent linear pattern with increasing temperature (Table 4). The magnitude of these increases declines in a downstream direction (cf. Lancang vs Mekong 1; Table 4). In the downstream part of the Mekong (sub-catchments 9–13), annual precipitation declines for all scenarios. The magnitude of these reductions increases with prescribed warming. There is also a downstream trend, so that whilst the maximum change in annual precipitation over the Se Kong (sub-catchment 9) is -3.2%, for Mekong 3 it is -6.7%. In the central Mekong (sub-catchments 5–8), annual precipitation responds in a non-linear way to increased prescribed warming (as a result of differing linear seasonal trends – see following paragraph and Figure 9). As Table 4 illustrates for the Mun (sub-catchment 6), annual precipitation initially declines with rising temperature, but later increases, such that for the 5 °C and 6 °C scenarios annual

precipitation is above the baseline. However, in all the scenarios, the magnitude of the changes is small (< ±1%). The same pattern is evident for Chi, Chi-Mun and Mekong 2.

For any given sub-catchment and month, precipitation changes linearly with increasing global mean temperature (Figure 9). There is, however, a downstream trend in the inter-seasonal pattern of precipitation change, as the number of months in which precipitation increases declines from north to south. For example, over the Lancang, precipitation increases in every month except April (Figure 9). The largest percentage changes occur in May–June and September–October, either side of the wettest months. By Mekong 1, increases in precipitation are limited to five months (in particular May–June but also September–October and December). Precipitation in the wettest baseline months (June–July) is reduced, although the extension of the wet season on either side of these two months results in the overall increase in annual precipitation, albeit of a smaller magnitude to the Lancang. For the four central sub-catchments, increasing precipitation is restricted to four months. Relatively large gains in precipitation are concentrated in the early part of the monsoon season. In the southernmost sub-catchments (e.g. Mekong 3), late monsoon precipitation declines, and increases in monthly totals are limited to May and June. The magnitudes of these increases are considerably smaller than those experienced in these months further upstream (e.g. May increase for the 1° C and 6 C °scenarios are 2.3% and 13.8%, respectively).

Throughout all the sub-catchments, annual PET increases linearly with prescribed warming (Table 4). Magnitudes of these changes are, in general, larger in the southern (warmer) part of the catchment compared to the northern (cooler) sub-catchments. PET increases throughout the year with, in most cases, a relatively constant climate change signal for each month (Figure 9). A notable exception is the elevated PET for April in some sub-catchments (e.g. Mekong 1), especially for the larger increases in temperature. In addition, percentage changes

in PET early and late in the year over some northern sub-catchments (e.g. the Lancang) are larger than those in summer due to the larger changes in temperature in these months. Absolute values of PET at this time of year remain, however, relatively low.

3.3.2. Changes in river flow

Values of the mean, Q5 and Q95 discharges for eight gauging stations for the baseline and the percentage changes in these discharges for each of the 1–6 °C, HadCM3 scenarios are shown in Table 6. Figure 10 provides the corresponding baseline and scenario river regimes. The eight gauging stations are the same as those used to present results for the 2 °C, seven GCM scenarios, and are representative of gauging stations for which results are not shown.

Changes in mean discharge for the 1–6 °C, HadCM3 scenarios follow the same geographical pattern as changes in annual precipitation. Mean discharge at the three upstream gauging stations increases linearly with prescribed warming (Table 6). This suggests that increases in precipitation more than compensate for higher PET. In most cases, mean monthly discharge increases throughout the year, with the magnitude of the increase rising with degree of prescribed warming (Figure 10). Exceptions are August for the 2 °C and 4 °C scenarios at all three stations and the 1 °C scenario at Luang Prabang and Vientiane, for which discharge declines slightly (<3%). This may be indicative of increases in evapotranspiration in this month outstripping enhanced precipitation. Table 6 shows that, in general, Q5 increases consistently with degree of prescribed warming, exceptions being the 1 °C scenario for Chiang Saen and Vientiane (modest decreases) and the 3 °C scenario at the second of these stations (a reduction in the magnitude of the increase compared to the 2 °C scenario). Peak flows characteristically remain in August, although for the 4 °C scenario at all three stations and the 6 °C scenario for Vientiane, the highest mean monthly discharge occurs a month later. The

higher dry season flows simulated cause Q95 to increase with the magnitude of prescribed warming, although the size of these increases declines with movement downstream.

Results for Mukdahan (and Nakhon Phanom, not shown) indicate larger mean flows as the magnitude of prescribed warming increases although, unlike further upstream, there is not a linear response to higher temperatures and changes for the 2 °C and 3 °C scenarios are similar (Table 6). Whilst discharges during the annual rise and recession increase with prescribed warming, peak flows in August and September are lower (Figure 10). These reductions are not related linearly to degree of warming, with the largest associated with the 4 °C scenario. This reflects the balance between lower precipitation and higher PET in these months. Whilst Q5 declines for the 1–4 °C scenarios, very modest increases result from the warmest scenarios. Higher dry season flows cause Q95 to increase with prescribed warming. These increases are sustained by flows from upstream rather than local runoff, as precipitation over the Mekong 1 sub-catchment declines as PET increases (Figure 9). The downstream reduction in the magnitude of increases in low flows continues (Table 6).

A similar pattern of change is evident at Pakse, although a decline in the magnitude of increases in mean discharge for the 3 °C scenario and very similar changes for the 2 °C and 4 °C scenarios interrupt the progressive increase with prescribed warming (Table 6). Changes are an order of magnitude lower than those further upstream. Mean monthly discharge during the annual rise and recession are still higher than for the baseline, although the size of these changes is also smaller (Figure 10). Mean discharge in August and September declines progressively with prescribed warming. The largest reductions occur in August, so that for the warmest scenario peak discharge occurs in September. Q5 declines for all scenarios, although not following a linear trend. Modest increases in dry season discharge result in higher Q95 discharges, although the downstream reduction in the magnitude of these changes continues.

Results for the Mun at Ubon, which flows into the Mekong just upstream of Pakse, are representative of the impacts of modest changes in annual precipitation coupled with large increases in PET over this part of the catchment. Mean flow declines consistently with degree of prescribed warming (Table 6). Changes are, in percentage terms, as large as those experienced at upstream gauging stations, albeit of an opposite direction. Particularly large reductions in discharge occur in months with the highest baseline flows (Figure 10), accounting for the further declines in peak flows in the Mekong at Pakse. Small increases in mean monthly discharge are limited to August (the 1 °C scenario) and June–July (3 °C–6 °C scenarios). Declines in discharge throughout most of the year, in particular during the annual recession and subsequent dry season, demonstrate that increases in discharge within the main Mekong at this time are dependent upon enhanced flows from upstream.

For gauging stations in the lower parts of the Mekong, a consistent pattern of changes in discharge is evident. Contributions from lower tributaries decline in a similar way to those described for Ubon. Mean discharge at the four stations on the lower Mekong therefore declines with prescribed warming and movement downstream (Table 6). Changes in the river regime are characterised by further reductions in peak discharges that are very slightly larger as the magnitude of prescribed warming increases (Figure 10). Whilst for the 1 °C and 2 °C scenarios mean monthly discharge declines in June and then between August and October, declines occur throughout the period June–October for the warmer scenarios. The month with the highest mean monthly discharge shifts from August to September for the most extreme (6 °C) scenario at all four gauging stations (and for the 4 °C scenario for Phnom Penh). The Q5 discharges decline at all four gauging stations, with the magnitude of these reductions initially increasing with prescribed warming, but showing less variability between the 3 °C and 6 °C scenarios (Table 6). Figure 10 shows very modest increases in dry season flows at Kratie and

Phnom Penh (repeated at Stung Treng and Kompong Cham) and as a result the values of Q95 increase. These increases are smaller compared to those for gauging stations upstream and are again the result of enhanced runoff in upstream parts of the catchment as opposed to local runoff at this time of year. There is less variability in these changes between prescribed warming scenarios except for the two extremes cases (the 1 °C and 6 °C scenarios).

Figure 11 shows percentages changes in mean annual discharge for four gauging stations resulting from the 1–6 °C, HadCM3 scenarios as well as those which result when one of each of the three meteorological inputs are modified in turn whilst retaining baseline values for the other two. It confirms the dominant influence of change in precipitation over upstream parts of the catchment (e.g. Chiang Saen). Consistent increases in precipitation with prescribed warming far outweigh increases in PET and are responsible for progressive increases in mean discharge. Further downstream, changes in discharge due to precipitation are smaller and begin to approximate those due to PET (e.g. Mukdahan and especially Phnom Penh). For tributaries in the south of the catchment in which discharge is not dominated by flows from upstream parts of the main Mekong, changes in PET exert a much larger influence (e.g. the Mun at Ubon). Results show that mean discharge is relatively insensitive to changes in temperature (excluding its influence upon PET), especially in lower parts of the catchment.

3.3.3. Comparison of MIKE SHE results with SLURP and Mac-PDM.09

Percentage changes in mean discharge (runoff for Mac-PDM.09) at six gauging stations (three for SLURP) for each of the 1–6 °C, HadCM3 scenarios, as simulated by the three hydrological models, are shown in Figure 12. Just as MIKE SHE demonstrates a spatially variable response of river flow to these scenarios, the inter-model differences in the discharge (runoff) climate change signal also vary throughout the catchment. The systematic increase in mean discharge

with magnitude of warming that occurs from Chiang Saen to middle parts of the catchment (Nakhon Phanom) for MIKE SHE are repeated for Mac-PDM.09 and probably SLURP, although results are limited to Chiang Saen. However, the magnitude of these changes varies between hydrological models. The smallest changes are associated with SLURP, at Chiang Saen ranging between +1.6% and +19.8% for the 1 °C and 6 °C scenarios, respectively. On average, the changes simulated by MIKE SHE are just over twice as large as those for SLURP, although the very small change for the 1 °C scenario for SLURP skews this value. In contrast, much larger increases in mean runoff are simulated by Mac-PDM.09 (range for Chiang Saen: +21.1% to +120.4%). On average, these are 4.2 and 8.0 times as large as those simulated by MIKE SHE and SLURP, respectively. The same pattern is repeated at Vientiane and Nakhon Phanom. The magnitude of increases in runoff declines in a downstream direction for Mac-PDM.09, just as they do for MIKE SHE (from a 120.4% increase at Chiang Saen to 48.5% at Nakhom Phanom).

Results for Ubon demonstrate that all three hydrological models respond in a similar way to the generally lower precipitation and consistently higher PET as prescribed warming increases (Figure 12). The order of magnitude of the resulting declines in mean discharge (runoff) is, however, different to the increases in the upper Mekong. MIKE SHE produces the largest reductions, whilst the smallest result from Mac-PDM.09, with the exception of the 2 °C scenario (SLURP>MIKE SHE). Reductions simulated by MIKE SHE are, on average, just under twice as large as the declines from Mac-PDM.09. The discharge reductions for SLURP are between those of these two models and are generally closer to those of Mac-PDM.09.

Differences in the magnitude and direction of flow changes in the upper and middle sections of the Mekong are responsible for the variable responses of the three hydrological models at downstream gauging stations on the Mekong (Figure 12). Whilst mean discharge simulated by MIKE SHE continues to increase, albeit not consistently with prescribed warming, results for

SLURP at Pakse demonstrate a variable response. Mean discharge declines for all but the 4 °C scenario. However, the largest decline is associated with the 3 °C scenario and the smallest with the 6 °C scenario. In contrast, the much larger increases in runoff upstream which are simulated by Mac-PDM.09 ensure that mean runoff at Pakse continues to increase with prescribed warming, despite reductions in runoff from downstream sub-catchments. The magnitude of the increases in mean runoff does, however, continue to decline in a downstream direction. The largest increase (6 °C scenario) is 21.3% compared to 48.5% for Nakhom Phanom. This trend continues further downstream so that whilst Mac-PDM.09 runoff at Phnom Penh increases with prescribed warming, the largest increase is only 6.0%. In contrast, the smaller increases in discharge from upstream catchments, coupled with the largest declines in discharge from southern sub-catchments, results in the previously reported declines in mean discharge at Phnom Penh that are simulated by MIKE SHE. The magnitude of these declines almost mirrors the increases simulated by Mac-PDM.09.

Mean monthly discharge (runoff for Mac-PDM.09) expressed as a percentage of the annual total is shown in Figure 13 for five (three for SLURP) gauging stations for the baseline and each 1–6 °C, HadCM3 scenario. Results for Nakhon Phanom are representative of those for Vientiane (not shown). Whilst for Chiang Saen, SLURP shows increased significance of flows during the first months of the year and the start of the annual rise, both MIKE SHE and Mac-PDM.09 show only modest changes at these times. Results for both MIKE SHE and SLURP do, however, show a smaller concentration of the total annual discharge during the peak season (August and September), with the monthly percentages declining with magnitude of prescribed warming. Conversely, both models show small increases (of greater magnitude with degree of prescribed warming) in the proportion of total annual discharge that occurs during the recession period. In contrast, Mac-PDM.09 simulates a consistently increasing

concentration of total annual runoff during the peak season (June–October) with prescribed warming and a subsequent decline in the significance of recession flows.

At Nakhon Phanom, results for MIKE SHE and Mac-PDM.09 are broadly in agreement. Smaller proportions of the annual total discharge / runoff occur in peak months of August and September. Both models indicate some increase in the significance of flows during the annual rise, whilst a noticeable increase in the October percentage is evident for Mac-PDM.09. In all cases, the magnitude of changes increases with prescribed warming. Similar broad agreement is evident between the three hydrological models for Pakse and between MIKE SHE and Mac-PDM.09 for Phnom Penh. Results for all the models at these stations repeat the reduced concentration of annual flows in the peak season and the enhanced importance of flows during May–July, the latter being particularly evident for SLURP. However, the enhanced percentages of annual runoff occurring in October (both stations) and the small reduction in the percentages for November (Phnom Penh) that are demonstrated for Mac-PDM.09 are not apparent for the other hydrological models. Results for Ubon for the three models also display similarities. All show increasing percentage of annual discharge / runoff during June and July followed by reductions for August and September for most scenarios. Whilst MIKE SHE and SLURP suggest that the proportion of total annual discharge occurring in the peak month remains largely unchanged, Mac-PDM.09 does suggest declines followed by increases for the following month that are replicated at gauging stations on the main Mekong.

4. Discussion

4.1. MIKE SHE model performance

The MIKE SHE model of the Mekong was developed using a combination of physically based, spatially distributed process descriptions alongside relatively simple conceptual, semi-distributed approaches appropriate for such a large catchment. Much of the data employed was taken from the earlier SLURP model (Kingston *et al.*, 2011). However, the use of observed discharge data from 12 gauging stations instead of the three employed by Kingston *et al.* (2011) provides a more robust calibration and assessment of model performance. This includes the extension of model results further downstream as well as greater confidence in the model's ability to simulate discharge through the catchment. Model performance for the 30 year calibration period is generally classified as "excellent", especially for gauging stations on the main Mekong upstream of and including Kratie. Performance statistics are superior to those obtained for the SLURP model using the same calibration period and compare very favourably with previous models of the Mekong (Hapuarachchi *et al.*, 2008; Västilä *et al.*, 2010). The performance of the model for the calibration period is weaker for gauging stations in the lowest part of the catchment (although it is generally still classified as "very good" or "fair"), but this may be related to the shorter (10–13 years) discharge records. Model performance for the two tributaries draining the Korat Plateau (the Chi and Mun) is notably poorer, echoing the results for SLURP, although it is still superior to those of this earlier study.

Model performance for the shorter validation period is generally classified as "very good" (some statistics retain the "excellent" classification), although mean discharge is consistently underestimated. This may be due to changes in the catchment not represented within the model. A number of dams have been constructed with, for example, the Manwan hydropower dam on the Lancang being completed during the validation period. Lu and Siew (2006) examined the effects of three Chinese dams built in the 1990s. They showed that whilst they had some impacts on seasonality of flows, there was no consistent impact on annual discharges since the hydropower dams are non-consumptive (apart from relatively small

evaporative losses). Alternatively, discharge underestimation may be related to land cover change. Deforestation within the Mekong has resulted from rapid economic development (Nobuhiro *et al.*, 2008) and has compounded earlier land cover change resulting from conflict (Lacombe *et al.*, 2010). However, in the absence of time series of vegetation cover (e.g. Delgado *et al.*, 2010), land cover remains constant through the calibration and validation periods, an approach also adopted by Kingston *et al.* (2011). Land cover change can, however, significantly impact runoff by altering evapotranspiration rates (Brown *et al.*, 2005). Large-scale forest clearance can increase runoff (Bruijnzeel, 2004), and over parts of the Mekong variations in rainfall-runoff relationships have been attributed to land cover modifications (Lacombe *et al.*, 2010). Initial exploratory experiments in which MIKE SHE grid squares specified as the three types of forest were progressively changed to agriculture caused discharge to increase. Discharge overestimation in the most extreme case was of a similar magnitude of (and in some cases exceeded) underestimation in the validation period. Detailed assessments of the impact of land cover change would merit further exploration using the MIKE SHE model. Similarly, inclusion of the extant and planned dams within the MIKE 11 model could assess their impacts under baseline conditions and the climate change scenarios.

The use of the same data as employed in the SLURP model within MIKE SHE inevitably resulted in the adoption of some approaches that may have differed if the new model had been developed in isolation from this earlier study. In particular, alternative meteorological inputs and their spatial distribution may have been used. For example, different sub-catchments defined the meteorological inputs and saturated zone linear reservoirs (the former taken from SLURP and the latter being influenced by gauging station location and catchment topography). The same spatial distribution for both might instead have been used. This could have advantages for the Lancang, which extends over a relatively large latitudinal range and has a wide range of elevations, but is represented by one meteorological input sub-

catchment (and three saturated zone linear reservoirs). Precipitation and temperature lapse rates result in some spatial variation in meteorological inputs, but the division of this large sub-catchment into smaller units could more properly account for this variation. Alternatively, meteorological inputs could be distributed using the 0.5° × 0.5° grid employed within these datasets. This would be analogous to changing inputs from station-based records (a single time series applied to a relatively large area) to gridded datasets. As demonstrated by previous research, this would likely require recalibration of the model (e.g. Mileham *et al.*, 2008; Xu *et al.*, 2010), but would enable the inclusion of smaller scale variations in meteorological inputs under both baseline conditions and the climate change scenarios.

Time series of precipitation used in the MIKE SHE model were derived from the UDel dataset, as adopted in the SLURP model. This followed initial difficulties in calibrating SLURP using CRU precipitation (Kingston *et al.*, 2011). UDel is derived from fewer meteorological stations than CRU and it is possible that explains the relatively poor performance of MIKE SHE for the Chi and Mun sub-catchments. Recalibration of the model using this alternative precipitation dataset and the assessment of its impact on scenario discharge could provide an extension of the current study. Similarly, initial attempts to calibrate the SLURP model employed the more data-intensive Penman-Monteith PET method, with all input data deriving from the CRU dataset (Kingston *et al.*, 2011). Model performance using these PET data was not satisfactory and it was argued that this might result from the additional requirement for humidity, wind speed and net radiation data. These data are typically less reliable in gridded datasets as a result of measurement difficulties and limited number of meteorological stations, especially for wind speed and net radiation (New *et al.*, 1999). As a result, the less data intensive Linacre PET was used and so was adopted for the MIKE SHE model. Previous research has, however, shown that different PET methods produce different climate change signals (e.g. Kingston *et al.*, 2009), with implications for climate change assessments of catchment-scale water

resources (e.g. Kay and Davies, 2008; Bae *et al.*, 2011). The implications of this additional source of uncertainty could be addressed using the MIKE SHE model, through its recalibration using alternative PET methods and subsequent simulation of the climate change scenarios.

The disconnect between daily meteorological inputs and observed discharge data used in model calibration results from using monthly precipitation totals and mean temperature and their disaggregation to a daily resolution using a stochastic weather generator. Although autocalibration routines (which evaluated objective functions at a time step of 48 hours) provided generally good performance, it was improved through manual modifications of parameters and the aggregation of observed and simulated discharge to mean monthly flows. This approach prevents the selection of a range of parameter sets close to the autocalibration optimum that could be used to assess equifinality-related uncertainty in climate change impacts on river discharge. Future research could employ alternative external autocalibration (e.g. PEST; Doherty, 2010), enabling the evaluation of objective functions at a monthly time step. Definition of multi-site objective functions based on comparisons of observed and simulated discharge at more than one gauging station (as opposed to sequential calibration in a downstream direction) could facilitate model parameter set selection along the Pareto front, as described by Madsen (2003), for subsequent climate change scenario simulation.

4.2. Climate change impacts on river flow simulated by MIKE SHE

Results from the scenarios associated with a 2 °C increase in global mean temperature indicate considerable uncertainty in Mekong discharge as simulated by MIKE SHE between the seven GCMs. Inter-CGM differences are predominantly driven by differences in precipitation. For some GCMs (CCCMA and NCAR), mean discharge increases throughout the catchment, for others (CSIRO and IPSL) discharge declines at all gauging stations. Results for

three GCMs indicate changes that depend upon location within the catchment. Declines in mean discharge occur in the upstream for MPI, whilst further downstream discharge increases. The reverse trend is evident for HadGEM1. For HadCM3, increases in mean discharge extend from upstream to central parts of the catchment whilst discharge declines at the lowest gauging stations. The spatial pattern for HadCM3 remains the same for increases in global mean temperature of between 1 °C and 6 °C, with the magnitude of changes generally increasing with higher temperatures except in central parts of the catchment. Upstream changes are driven by increases in precipitation, whilst with movement further downstream, the influence of higher precipitation is equalled and then exceeded by the impact of higher PET, especially for the most extreme warming scenarios.

Although MIKE SHE demonstrates differences in river flow between different GCMs for the same climate change scenario and for alternative scenarios for the same GCM, an evaluation of the uncertainty in the environmental or water resources implications of these differences would merit further research. For example, approaches such as the Indicators of Hydrological Alteration (IHA), which defines ecologically appropriate limits of hydrological change (Richter *et al.*, 1996, 1997), could provide a method for assessing uncertainty in the impacts of changes in flow regime upon environmental flow conditions within the Mekong. More applied research, such as that based on these ecological impacts, is required before the concept of 2 °C as a threshold for dangerous climate change can be validated.

4.3. Comparison of climate change impacts between hydrological models: GCM- versus hydrological model-related uncertainty

Comparison of climate change scenario results from MIKE SHE with those from an alternative catchment hydrological model (SLURP) and the Mac-PDM.09 global hydrological model

provides an opportunity to assess the magnitude of uncertainty associated with the use of alternative hydrological models. As previously noted, this source of uncertainty is less frequently considered in hydrological impact assessments compared to those associated with alternative GCMs (Prudhomme and Davies, 2009). This study demonstrates that, in accordance with other investigations (Dibike and Coulibaly, 2005; Haddeland *et al*., 2011; Hagemann *et al*., 2012), hydrological model-related uncertainty should not be ignored. However, results suggest that, in general, climate model uncertainty is larger than that associated with the choice of hydrological model. Although results for the different GCMs demonstrate both increases and decreases in mean discharge (runoff for Mac-PDM.09), the direction of change simulated by each of the hydrological models for a particular gauging station is predominantly the same (differing for only three out of 42 gauging station / GCM combinations). Where the direction of the mean river flow climate change signal differs between hydrological models, the magnitude of change is relatively small. In most cases, the smallest changes are associated with SLURP and the largest with Mac-PDM.09. The larger climate change signal for Mac-PDM.09 is most evident in those scenarios where runoff is projected to increase, especially at upstream gauging stations. The HadCM3 GCM, in particular, results in much larger changes for the global hydrological model compared to the two catchment models.

Despite these differences, there are similarities in the distribution of river flows through the year in each of the hydrological models. Many of the changes in these distributions simulated by MIKE SHE for the climate change scenarios are replicated by Mac-PDM.09, although the amplitude of the annual cycle is greater for the latter model. Similarities in the seasonal flow distribution from the SLURP model and both MIKE SHE and Mac-PDM.09 are also evident. In particular, common features occur in the results for lower gauging stations, where the

influence of the earlier rise in the annual hydrograph in the far north that is simulated by SLURP, but less so by MIKE SHE and Mac-PDM.09, has diminished.

Quantification of the relative uncertainty associated with choice of GCM and hydrological model can be provided using the approach of Gosling *et al.* (2011a). The greatest absolute differences in the mean annual discharge (runoff) climate change signal between any two GCMs for the 2 °C scenarios for Pakse as simulated by MIKE SHE, SLURP and Mac-PDM.09 are 26.7%, 24.3% and 31.5%, respectively. In comparison, the largest absolute MIKE SHE–SLURP difference in the climate change signal for this station for any GCM is 4.7%. The corresponding figures for MIKE SHE–Mac-PDM.09 and SLURP–Mac-PDM.09 comparisons are 7.0% and 10.0%, respectively. This suggests that GCM-related uncertainty is between 2.5 and nearly six times that associated with choice of hydrological model.

The analysis of Gosling *et al.* (2011a) was limited to Pakse, the furthest downstream gauging station simulated by SLURP. By extending the inter-hydrological model analysis to other stations, it is possible to identify spatial differences in the relative uncertainty due to choice of GCM and hydrological model. Whilst for downstream gauging stations (Phnom Penh and Ubon), the absolute differences in the climate change signal for the different hydrological models for any GCM are similar to those for Pakse, further upstream, differences between results for the two catchment models and Mac-PDM.09 are larger. At Chiang Saen, the largest absolute MIKE SHE–SLURP difference in the climate change signal for any GCM is 7.9%. The corresponding figures for comparisons between MIKE SHE–Mac-PDM.09 and SLURP–Mac-PDM.09 are 31.8% and 38.5%. These compare to the largest absolute differences in climate change signal between any two GCMs simulated by MIKE SHE, SLURP and Mac-PDM.09 of 29.9%, 18.8% and 43.3%, respectively. Inter-hydrological model range in climate change signal when comparing catchment and global models is therefore of a similar or even larger

magnitude than that associated with different GCMs. This result is predominantly due to the large increases in mean runoff simulated by Mac-PDM.09 for three scenarios, and in particular HadCM3. Excluding this GCM from the inter-hydrological model comparisons lowers the largest absolute difference in mean discharge climate change signal for any GCM to 11.1% and 13.6% for MIKE SHE–Mac-PDM.09 and SLURP–Mac-PDM.09, respectively. As noted above, however, the direction of change for each GCM is the same for the three hydrological models.

Differences between results of Mac-PDM.09 and the two catchment models for the HadCM3 GCM is especially evident for the 1–6 °C scenarios and has implications for direction of change in mean runoff. Whilst both MIKE SHE and Mac-PDM.09 simulate increases in mean discharge / runoff at upstream gauging stations (with similar, albeit smaller, increase predicted by SLURP at Chiang Saen), towards the downstream end of the catchment the direction of change for the two models almost mirror one another (small increases for Mac-PDM.09, declines of equal magnitude for MIKE SHE). The much larger upstream increases simulated by Mac-PDM.09 effectively drown out the influence of declining contributions from tributaries in the southern part of the catchment that are common to all three hydrological models. As such, differences between the results for the two catchment hydrological models and Mac-PDM.09 for HadCM3 are a result of the spatially variable changes in projected climate: relatively large (compared to other GCMs) upstream increases in precipitation and progressively larger reductions in precipitation in a downstream direction.

In contrast to the HadCM3 scenarios, differences between catchment and global hydrological models are smaller where a predominantly uniform change in climate is projected by a GCM (increasing precipitation across the catchment: e.g. CCCMA, MPI and NCAR; declining precipitation over all, or most, sub-catchments: e.g. CSIRO, ISPL). Results from this study suggest that although the global hydrological model may provide a useful tool in assessing

likely changes in runoff at the individual catchment scale, care should be taken in situations such as those presented by the HacCM3 scenarios where spatially variable climate change signals are projected for a catchment. Differences in modelled hydrological response from linear changes in monthly climate introduce uncertainty into the identification of thresholds for “dangerous climate change”.

Although a precise identification of the reasons for the differences in climate change signals from the three hydrological models is difficult due to their inherently different structures and process representations (Table 1), it is possible to highlight some factors which may influence the different responses of simulated discharge / runoff. For example, the previously noted greater amplitude of the annual runoff cycle simulated by Mac-PDM.09 for the baseline and each scenario when compared to discharge results from MIKE SHE (and, where available, SLURP) is probably due to the absence of routing of runoff within Mac-PDM.09. Consequently runoff generated in the far north of the catchment is included within the total runoff for that month at a gauging station that may be hundreds or thousands of kilometres downstream.

Other differences may result from the spatial resolution and distribution of process computation. For example, the MIKE SHE model undertakes process calculations, with the exception of the saturated zone (for which the linear reservoirs are employed), for all cells within the 10 km × 10 km computational grid. The spatial distribution of catchment characteristics at this scale is therefore represented, and there is the potential for exchange between grid cells though processes such as overland flow. Similarly, water balance calculations within Mac-PDM.09 are undertaken for each 0.5° × 0.5° cell although, as described above, each cell is treated as an independent catchment and there is no exchange between neighbouring cells. SLURP, in contrast, evaluates vertical balances for a relatively small number of elements, with results being aggregated at the sub-catchment scale.

Linked to the approach used to distribute process calculations and catchment characteristics is the distribution of meteorological inputs. MIKE SHE and SLURP employed the same sub-catchments to define the distribution of meteorological inputs (albeit with spatial variation in MIKE SHE being induced through the inclusion of lapse rates), whereas Mac-PDM.09 employed the 0.5° × 0.5° grid used within the gridded meteorological datasets. As discussed above, the latter is more likely to represent true spatial variability over the catchment, especially for large sub-catchments such as the Lancang. The application of alternative approaches to distribute meteorological inputs has been highlighted as a potential development of the current study.

A potential cause of Mac-PDM.09 simulating larger increases in mean runoff at upstream gauging stations for the HadCM3 1–6 °C scenarios, as well as for the 2 °C scenarios for other GCMs for which such increases occur, may be related to the PET methods employed by the three hydrological models. Mac-PDM.09, which was not specifically calibrated for the Mekong since it is typically applied to assess runoff at the continental to global scale, uses Penman-Monteith PET. In contrast, Kingston *et al.* (2011) selected Linacre PET for the SLURP model and this dataset was employed in the MIKE SHE model. As discussed previously, Linacre PET was used following unsuccessful attempts to calibrate SLURP using Penman-Monteith PET. The use of the latter PET method resulted in significant over-estimation of discharge. Evaluation of mean annual Penman-Monteith PET using the CRU TS 3.0 dataset for each of the meteorological input sub-catchments shows that on average baseline Penman-Monteith PET is 71.6% of Linacre PET. The mean increase in annual Linacre PET for the 2 °C HadCM3 scenario for all the sub-catchments is 14.4% compared to 8.9% for Penman-Monteith. This pattern is repeated for the other scenarios. Therefore, although Mac-PDM.09 is responding to the same changes in precipitation, absolute PET and scenario increases are smaller. It is likely

that this results in the larger increases in mean Mac-PDM.09 runoff for those scenarios in which precipitation increases. This sensitivity to alternative PET methods, previously demonstrated for Mac-PDM.09 by Gosling and Arnell (2011), strengthens the argument for using the MIKE SHE model to evaluate this additional source of uncertainty upon climate change projections of Mekong River discharge.

This study has demonstrated that GCM-related uncertainty in climate change projections for the Mekong is predominantly larger than that related to the use of three alternative hydrological models. The latter, however, is not negligible, and in some cases hydrological model related-uncertainty is of a similar magnitude to GCM-related uncertainty. GCM-related uncertainty could be addressed by the development of GCM reliability ratings using comparisons between simulated and observed climate (e.g. Perkins *et al.*, 2007; Maxino *et al.*, 2008; Ghosh and Mujumdar, 2009). This would be particularly valuable since a number of studies have suggested GCM shortcomings in the representation of monsoon climate (e.g. Kang *et al.*, 2002; Waliser *et al.,* 2003; Wang *et al.*, 2004). Evaluation of GCM performance is beyond the scope of the current study. However, an investigation by Kripalani *et al.* (2007) has demonstrated considerable differences in the ability of 22 GCMs, including the seven employed in this study, to reproduce the annual monsoon cycle. CCCMA, MPI and NCAR simulated mean monthly precipitation that was similar in terms of shape and magnitude to the observed derived from the Climate Prediction Center Merged Analysis Precipitation (CMAP) dataset (Xie and Arkin, 1997). HadGEM1 reproduced the annual cycle but underestimated precipitation amounts whilst CSIRO and HadCM3 simulated peak precipitation a month later than the observed. ISPL was one of three models that did not accurately reproduce the annual monsoon precipitation cycle. This earlier investigation, however, considered the south Asian region, with the region of interest only just extending into the far western part of the upper Lancang sub-catchment. A similar GCM / observed

precipitation comparison over southeast Asia would be required to confirm whether the relative performance of the different GCMs extended to the Mekong catchment.

5. Conclusions

The MIKE SHE model of the Mekong, which utilises a combination of physically based, spatially distributed process descriptions and simpler conceptual, semi-distributed approaches, successfully simulates river discharge through the catchment. Model performance is generally classified as “excellent” or “very good” and is superior to the SLURP model from which most model data is derived. The MIKE SHE model also compares very favourably with previous hydrological models of the Mekong.

The simulation of two sets of climate change scenarios reveals considerable uncertainty in projected river discharge. Whilst results for a 2° C increase in global mean temperature using projections from two GCMs indicate increases in discharge throughout the catchment, another two GCMs produce consistent decreases in Mekong discharge. Results for a further three GCMs indicate that the direction of change in discharge varies spatially through the catchment. Variations in the results for the different GCMs are largely driven by differences in precipitation. Scenarios associated with one GCM (HadCM3) and increases in global mean temperate of between 1° C and 6° C demonstrate consistent increases in discharge in upstream parts of the catchment, where the climate change signal is dominated by increasing precipitation. The climate change signal in downstream parts of the catchment is more strongly influenced by increasing PET, which outweighs the impacts of elevated upstream precipitation and results in consistent reductions in discharge for warmer scenarios.

A comparison of results for the two sets of climate change scenarios simulated by MIKE SHE, the SLURP semi-distributed conceptual catchment model and the Mac-PDM.09 global hydrological model demonstrates that hydrological model-related uncertainty should not be ignored. However, in most cases the magnitude of this uncertainty is less than GCM uncertainty. The direction of change in mean runoff for any GCM from the 2 °C scenario set is predominantly the same across the hydrological models, whilst similar features are evident in changes in the seasonal distribution of flows. Mac-PDM.09 is, however, often associated with larger changes than MIKE SHE and SLURP, especially where mean flow is projected to increase.

Over upstream parts of the catchment, differences between the catchment and global hydrological models are of a similar magnitude to those associated with different GCMs. This is probably due to alternative PET methods used within the models. Larger increases in runoff upstream for Mac-PDM.09 have implications for the direction of change further downstream, especially for scenarios (in particular HadCM3) where the nature of projected changes in climate varies across the catchment. Whilst the global hydrological model therefore provides a useful tool for assessing impacts of climate change on runoff at the individual catchment scale and, in particular, for quantifying climate model uncertainty in situations where a catchment model is not available or where time or resources are inadequate to develop such a model, care should be taken in some circumstances such as with applying the model to individual sub-catchments with large distinct spatial variations in baseline or projected future climate. Moreover, the application of any global hydrological model to the sub-catchment scale should be approached carefully, since these models are inherently intended for application across larger spatial domains.

Possible extensions of this research could include rigorous assessments of the impacts of past and future land cover change upon runoff. The implications of using other precipitation datasets and different PET methods within the MIKE SHE model, as well as alternative approaches of spatially distributing these meteorological inputs, upon projected river flow for the same climate change scenarios would provide additional insights into hydrological model-related uncertainty. Finally, assessments of the implications of uncertainty in the hydrological projections presented in the current study for ecological conditions would be a valuable next step for research on climate change and the Mekong River.

Acknowledgements: The present study develops earlier research supported by a grant from the UK Natural and Environmental Research Council under the Quantifying and Understanding the Earth System (QUEST) programme (Ref. NE/E001890/1). Geoff Kite provided the data employed in the SLURP model. ClimGen climate scenarios were generated by Tim Osborn at the Climatic Research Unit of the University of East Anglia. The development of the MIKE SHE model benefitted from discussions with Mike Butts and Douglas Graham. The final manuscript benefitted from comments from an Associate Editor and two anonymous reviewers.

References

Abbott, M.B., Bathurst, J.C., Cunge, J.A., O'Connell, P.E., Rasmussen, J., 1986a. An introduction to the European hydrological system – Système Hydrologique Européen, SHE. 1 History and philosophy of a physically-based distributed modelling system. J. Hydrol. 87, 45–59.

Abbott, M.B., Bathurst, J.C., Cunge, J.A., O'Connell, P.E., Rasmussen, J., 1986b. An introduction to the European hydrological system – Système Hydrologique Europeén, SHE. 2 Structure of a physically-based distributed modelling system. J. Hydrol. 87, 61–77.

Acreman, M.C., Blake, J.R., Mountford, O., Stratford, C., Prudhomme, C., Kay, A., Bell, V., Gowing, D., Rothero, E., Thompson, J.R., Hughes, A., Barkwith, A., van de Noort, R., 2012. Guidance on using wetland sensitivity to climate change tool-kit. A contribution to the Wetland Vision Partnership. Centre for Ecology and Hydrology, Wallingford.

Andersen, J., Refsgaard J.C., Jensen, K.H., 2001. Distributed hydrological modelling of the Senegal River Basin - model construction and validation. J. Hydrol. 247, 200–214.

Andréasson, J., Bergström, S., Carlsson, B., Graham, L.P., Lindström, G., 2004. Hydrological change: climate change impact simulations for Sweden. Ambio 33, 228-234.

Arnell, N.W., 1999a. The effect of climate change on hydrological regimes in Europe: a continental perspective. Glob. Environ. Change 9, 5–23.

Arnell, N.W., 1999b. A simple water balance model for the simulation of streamflow over a large geographic domain. J. Hydrol. 217, 314–335.

Arnell, N.W., 2003. Effects of IPCC SRES* emissions scenarios on river runoff: a global perspective. Hydrol. Earth Syst. Sci. 7, 619-641.

Arnell, N.W., Gosling, S.N., 2013. The impacts of climate change on river flow regimes at the global scale. J. Hydrol. Submitted.

Arnell, N.W., Osborn, T., 2006. Interfacing Climate and Impacts Models in Integrated Assessment Modelling, Tyndall Centre for Climate Change Research Technical Report 52. Tyndall Centre for Climate Change Research, Southampton and Norwich.

Arnold, J.G., Srinivasan, R., Muttiah, R.S., Williams, J.R., 1998. Large area hydrologic modeling and assessment part I: model development. J. Am. Water Resour. Assoc. 34, 73–89.

Bae, D.H., Jung, I.W., Lettenmaier, D.P., 2011. Hydrologic uncertainties in climate change from IPCC AR4 GCM simulations of the Chungju Basin, Korea. J. Hydrol. 401, 90–105.

Bates, B.C., Kundzewicz, Z.W., Wu, S., Palutikof, J.P. (Eds.), 2008. Climate Change and Water, Technical Paper of the Intergovernmental Panel on Climate Change. IPCC Secretariat, Geneva.

Brown, A.E., Zhang, L., McMahon, T.A., Western, A.W., Vertessy, R.A., 2005. A review of paired catchment studies for determining changes in water yield resulting from alterations in vegetation. J. Hydrol. 310, 28–61.

Bruijnzeel, L.A., 2004. Hydrological functions of tropical forests: not seeing the soil for the trees. Agric. Ecosyst. Environ. 104, 185–228.

Butts, M.B., Payne, J.T., Kristensen, M., Madsen, H., 2004. An evaluation of the impact of model structure on hydrological modelling uncertainty for streamflow simulation. J. Hydrol. 298, 242–266.

Carsel, R.F. and Parrish, R.S., 1988. Developing joint probability distributions of soil water retention characteristics. Water Resour. Res. 24, 755-769.

Chow, V.T., 1959. Open Channel Hydraulics. McGraw-Hill, New York.

Chun, K.P., Wheater, H.S., Onof, C.J., 2009. Streamflow estimation for six UK catchments under future climate scenarios. Hydrol. Res. 40, 96-112.

Clapp, R.B., Hornberger, G.M., 1978. Empirical equations for some soil hydraulic properties. Water Resour. Res. 14, 601–604.

Conway, D., Hulme, M., 1996. The impacts of climate variability and future climate change in the Nile Basin on water resources in Egypt. Int. J. Water Resour. Dev. 12, 277-296.

Dai, Z., Li, C., Trettin, C., Sun, G., Amatya, D., Li, H., 2010. Bi-criteria evaluation of the MIKE SHE model for a forested watershed on the South Carolina coastal plain. Hydrol. Earth Syst. Sci. 14, 1033–1046.

Delgado, J.M., Apel, H., Merz, B., 2010. Flood trends and variability in the Mekong river. Hydrol. Earth Syst. Sci. 14, 407–418.

Dibike, Y.B., Coulibaly, P., 2005. Hydrologic impact of climate change in the Saguenay watershed: comparison of downscaling methods and hydrologic models. J. Hydrol. 307, 145–163.

DHI, 2009. MIKE SHE Technical Reference. DHI Water and Environment, Hørsholm.

Doherty, J., 2010. PEST: Model-Independent Parameter Estimation User Manual, fifth ed. Watermark Numerical Computing, Brisbane.

Döll, P., Kaspar, F., Lehner, B., 2003. A global hydrological model for deriving water availability indicators: model tuning and validation. J. Hydrol. 270, 105–134.

Duan, Q., Sorooshian, S., Gupta, V., 1992. Effective and efficient global optimization for conceptual rainfall-runoff models. Water Resour. Res. 28, 1015–1031.

FAO, 1990. FAO-UNESCO Soil Map of the World: Revised Legend, World Soil Resources Report 60. Food and Agriculture Organization of the United Nations, Rome.

Feyen, L., Vázquez, R., Christiaens, K., Sels, O., Feyen, J., 2000. Application of a distributed physically-based hydrological model to a medium size catchment. Hydrol. Earth Syst. Sci. 4, 47–63.

Ghosh, S., Mujumdar, P.P., 2009. Climate change impact assessment: uncertainty modelling with imprecise probability. J. Geophys. Res. 114, D18113.

Gosling, S.N., 2012. The likelihood and potential impact of future change in the large-scale climate-earth system on ecosystem services. Environ. Sci. Policy. http://dx.doi.org/10.1016/j.envsci.2012.03.011

Gosling, S.N., Arnell, N.W., 2011. Simulating current global river runoff with a global hydrological model: model revisions, validation and sensitivity analysis. Hydrol. Process. 25, 1129–1145.

Gosling, S.N., Bretherton, D., Haines, K., Arnell, N.W., 2010. Global hydrology modelling and uncertainty: running multiple ensembles with a campus grid. Philos. Trans. R. Soc. A 368, 1-17.

Gosling, S.N., Taylor, R.G., Arnell, N.W., Todd, M.C., 2011a. A comparative analysis of projected impacts of climate change on river runoff from global and catchment-scale hydrological models. Hydrol. Earth Syst. Sci. 15, 279–294.

Gosling, S.N., Warren, R., Arnell, N.W., Good, P., Caesar, J., Bernie, D., Lowe, J.A., van der Linden, P., O'Hanley, J.R., Smith, S.M., 2011b. A review of recent developments in climate change science. Part II: the global-scale impacts of climate change. Prog. Phys. Geog. 35, 443–464.

Graham, D.N., Butts, M.B., 2005. Flexible, integrated watershed modelling with MIKE SHE, in: Singh V.P., Frevert, D.K. (Eds.), Watershed Models. CRC Press, Boca Raton, pp. 245–272.

Haddeland, I., Clark, C., Franssen, W., Ludwig, F., Voß, F., Bertrand, N., Folwell, S., Gerten, D., Gomes, S., Gosling, S.N., Hagemann, S., Hanasaki, N., Heinke, J., Kabat, P., Koirala, S., Polcher, J., Stacke, T., Viterbo, P., Weedon, G., Yeh, P., 2011. Multi-model estimate of the global water balance: setup and first results. J. Hydrometeorol. 12, 869–884.

Hagemann, S., Chen, C., Clark, D.B., Folwell, S., Gosling, S.N., Haddeland, I., Hanasaki, N., Heinke, J., Ludwig, F., Voß, F., Wiltshire, A. J., 2012. Climate change impact on available water

resources obtained using multiple global climate and hydrology models. Earth Syst. Dyn. Discuss. 3, 1321–1345.

Hammersmark, C.T., Rains, M.C., Mount, J.F., 2008. Quantifying the hydrological effects of stream restoration in a montane meadow, northern California, USA. River Res. Appl. 24, 735–753.

Hapuarachchi, H.A.P., Takeuchi, K., Zhou, M.C., Kiem, A.S., Georgievski, M., Magome, J., Ishidaira, H., 2008. Investigation of the Mekong River basin hydrology for 1980-2000 using the YHyM. Hydrol. Process. 22, 1246-1256.

Havnø, K., Madsen, M.N., Dørge, J., 1995. MIKE 11 – a generalized river modelling package, in: Singh, V.P (Ed.), Computer Models of Watershed Hydrology. Water Resources Publications, Englewood, pp. 733–782.

Henriksen, H.J., Troldborg, L., Højberg, A.J., Refsgaard, J.C., 2008. Assessment of exploitable groundwater resources of Denmark by use of ensemble resource indicators and a numerical groundwater–surface water model. J. Hydrol. 348, 224–240.

Henriksen, H.J., Troldborg, L., Nyegaard, P., Sonnenborg, T.O., Refsgaard, J.C., Madsen, B., 2003. Methodology for construction, calibration and validation of a national hydrological model for Denmark. J. Hydrol. 280, 52–71.

Huang, Y., Chen, X., Li, Y.P., Willems, P., Liu, T., 2010. Integrated modeling system for water resources management of Tarim River Basin. Environ. Eng. Sci. 27, 255–269.

Institute of Hydrology, 1988. Investigation of Dry Season Flows. Water Balance Study Phase 3. Report to the Interim Committee for Coordination of Investigations of the Lower Mekong Basin. Institute of Hydrology, Wallingford.

Ishidaira, H., Ishikawa, Y., Funada, S., Takeuchi, K., 2008. Estimating the evolution of vegetation cover and its hydrological impact in the Mekong River basin in the 21st century. Hydrol. Process. 22, 1395-1405.

Jackson, R.B., Canadell, J., Ehleringer, J.R., Mooney, H.A., Sala, O.E., Schulze, E.D., 1996. A global analysis of root distributions for terrestrial biomes. Oecologia 108, 389–411.

Jenkins, G.J., Murphy, J.M., Sexton, D.M.H., Lowe, J.A., Jones, P., Kilsby, C.G., 2009. UK Climate Projections: Briefing Report. Met Office Hadley Centre, Exeter.

Kang, I.S., Jin, K., Wang, B., Lau, K.M., Shukla, J., Krishnamurthy, V., Schubert, S.D., Waliser, D.E., Stern, W.F., Kitoh, A., Meehl, G.A., Kanamitsu, M., Galin, V.Y., Satyan, V., Park, C.K., Liu, Y., 2002. Intercomparison of the climatological variations of Asian summer monsoon precipitation simulated by 10 GCMs. Clim. Dyn. 19, 383–395.

Kay, A.L., Davies, H.N., 2008. Calculating potential evaporation from climate model data: A source of uncertainty for hydrological climate change impacts. J. Hydrol. 358, 221–239.

Kelliher, F.M., Leuning, R., Schulze, E.D., 1993. Evaporation and canopy characteristics of coniferous forests and grasslands. Oecologia 95, 153–163.

Kiem, A.S., Geogievsky, M.V., Hapaurachchi, H.P., Ishidaira, H., Takeuchi, K., 2005. Relationship between ENSO and snow covered area in the Mekong and Yellow River basins, in: Franks, S. W., Wagener, T., Bøgh, E., Bastidas, L., Nobre, C., and Galvão, C.O. (Eds.), Regional Hydrological Impacts of Climate Change – Hydroclimatic variability. IAHS Publ. 296. Wallingford, pp. 255-264.

Kiem, A.S., Ishidaira, H., Hapuarachchi, H.P., Zhou, M.C., Hirabayahi, Y., Takeuchi, K., 2008. Future hydroclimatology of the Mekong River basin simulated using the high-resolution Japan Meteorological Agency (JMA) AGCM. Hydrol. Process. 22, 1382-1394.

Kingston, D.G., Thompson, J.R., Kite, G., 2011. Uncertainty in climate change projections of discharge for the Mekong River Basin. Hydrol. Earth Syst. Sci. 15, 1459-1471.

Kingston, D.G., Todd, M.C., Taylor, R.G., Thompson, J.R., Arnell, N.W., 2009. Uncertainty in the estimation of potential evapotranspiration under climate change. Geophys. Res. Lett. 36, L20403.

Kite, G., 1995. The SLURP model, in: Singh, V.P. (Ed.) Computer models of watershed hydrology. Water Resources Publications, Colorado, pp. 521-562.

Kite, G., 2000. Developing a Hydrological Model for the Mekong Basin: Impacts of Basin Development on Fisheries Productivity. Working Paper 2. International Water Management Institute, Colombo.

Kite, G., 2001. Modelling the Mekong: hydrological simulation for environmental impact studies. J. Hydrol. 253, 1-13.

Kripalani, R.H., Oh, J.H., Kulkarni, A., Sabade, S.S. Chaudhari, H.S., 2007. South Asian summer monsoon precipitation variability: Coupled climate model simulations and projections under IPCC AR4. Theor. Appl. Climatol. 90, 133–159.

Kummu, M., Lu, X.X., Wang, J.J., Varis, O., 2010. Basin-wide sediment trapping efficiency of emerging reservoirs along the Mekong. Geomorphology 119, 181-197.

Kundzewicz, Z.W., Mata, L.J., Arnell, N.W., Döll, P., Kabat, P., Jiménez, B., Miller, K.A., Oki, T., Sen, Z., Shiklomanov, I.A., 2007. Freshwater resources and their management, in: Parry, M.L., Canziani, O.F., Palutikof, J.P., van der Linden, P.J., Hanson, C.E. (Eds.), Climate Change 2007: Impacts, Adaptation and Vulnerability. Contribution of Working Group II to the Fourth Assessment Report of the Intergovernmental Panel on Climate Change. Cambridge University Press, Cambridge, pp. 173–210.

Lacombe, G., Pierret, A., Hoanh, C.T., Sengtaheuanghoung, O., Noble, A.D., 2010. Conflict, migration and land-cover changes in Indochina: A hydrological assessment. Ecohydrology 3, 382–391.

Legates, D.R., Willmott, C.J., 1990. Mean seasonal and spatial variability in gauge-corrected, global precipitation. Int. J. Climatol. 10, 111–127.

Li, S.J., He, D.M., 2008. Water level response to hydropower development in the upper Mekong River. Ambio 37, 170-177.

Lu, X.X., Siew, R.Y., 2006. Water discharge and sediment flux changes over the past decades in the Lower Mekong River: possible impacts of the Chinese dams. Hydrol. Earth Syst. Sci. 10, 181–195.

Madsen, H., 2000. Automatic calibration of a conceptual rainfall-runoff model using multiple objectives. J. Hydrol. 235, 276–288.

Madsen, H., 2003. Parameter estimation in distributed hydrological catchment modelling using automatic calibration with multiple objectives. Adv. Water Resour. 26, 205–216.

Marshall, T.J., Holmes, J.W., Rose, C.W., 1996. Soil Physics, third ed. Cambridge University Press, Cambridge.

Matthews, J.H., Quesne, T.L., 2009. Adapting Water Management: A Primer on Coping with Climate Change. WWF Water Security Series 3, WWF-UK, Godalming.

Maxino, C.C., McAvaney, B.J., Pitman, A.J. and Perkins, S.E., 2007. Ranking the AR4 climate models over the Murray-Darling Basin using simulated maximum temperature, minimum temperature and precipitation. Int. J. Climatol. 28, 1097-1112.

McMichael, C.E., Hope, A.S., Loaiciga, H.A., 2006. Distributed hydrological modelling in California semi-arid shrublands: MIKE SHE model calibration and uncertainty estimation. J. Hydrol. 317, 307–324.

Meehl, G.A., Covey, C., Delworth, T., Latif, M., McAvaney, B., Mitchell, J.F.B., Stouffer, R.J., Taylor, K.E., 2007. The WCRP CMIP3 Multimodel Dataset: A new era in climate change research. Bull. Am. Meteorol. Soc. 88, 1383–1394.

Mekong River Commission (MRC), 2003. State of the Basin Report: 2003. Mekong River Commission, Phnom Penh.

Mileham, L., Taylor, R.G., Thompson, J.R., Todd, M.C., Tindimugaya, C., 2008. Impact of rainfall distribution on the parameterisation of a soil-moisture balance model of groundwater recharge in equatorial Africa. J. Hydrol. 359, 46–58.

Mitchell, T.D., Jones, P.D., 2005. An improved method of constructing a database of monthly climate observations and associated high-resolution grids. Int. J. Climatol. 25, 693–712.

Murphy, J.M., Sexton, D.M.H., Barnett, D.N., Jones, G.S., Webb, M.J., Collins, M., Stainforth, D.A., 2004. Quantification of modelling uncertainties in a large ensemble of climate change simulations. Nature 430, 768-772.

Nash, I.E., Sutcliffe, I.V., 1970. River flow forecasting through conceptual models. J. Hydrol. 10, 282–290.

Nawaz, N.R., Adeloye, A.J., 2006. Monte Carlo assessment of sampling uncertainty of climate change impacts on water resources yield in Yorkshire, England. Clim. Change 78, 257–292.

New, M., Hulme, M., Jones, P.D., 1999. Representing twentieth century space-time climate variability, Part I: Development of a 1961–1990 mean monthly terrestrial climatology. J. Clim. 12, 829–856.

Nijssen, B., O'Donnell, G.M., Hamlet, A.F., Lettenmaier, D.P., 2001. Hydrologic sensitivity of global rivers to climate change. Clim. Change 50, 143-175.

Nobuhiro, T., Shimizu, A. Kabeya, N., Tamai, K., Ito, E., Araki, M., Kubota, T., Tsuboyama, Y., Chann, S., 2008. Evapotranspiration during the late rainy season and middle of the dry season in the watershed of an evergreen forest area, central Cambodia. Hydrol. Process. 22, 1281–1289.

Nohara, D., Kitoh, A., Hosaka, M., Oki, T., 2006. Impact of climate change on river discharge projected by multimodel ensemble. J. Hydrometeorol. 7, 1076–1089.

Perkins, S.E., Pitman, A.J., Holbrook, N.J. and McAveney, B.J., 2007. Evaluation of the AR4 climate models' simulated daily maximum temperature, minimum temperature and precipitation over Australia using probability density functions. J. Clim. 20, 4356-4376.

Poff, N.L., Brinson, M.M., Day. Jr. J.W., 2002. Aquatic Ecosystems and Global Climate Change. Pew Center on Global Climate Change, Arlington.

Prudhomme, C., Davies, H., 2009. Assessing uncertainties in climate change impact analyses on the river flow regimes in the UK. Part 1: baseline climate. Clim. Change 93, 177–195.

Prudhomme, C., Jakoba, D., Svensson, C., 2003. Uncertainty and climate change impact on the flood regime of small UK catchments. J. Hydrol. 277, 1–23.

Refsgaard, J.C., Storm, B., Clausen, T., 2010. Système Hydrologique Europeén (SHE): review and perspectives after 30 years development in distributed physically-based hydrological modelling. Hydrol. Res. 41, 355–377.

Richter, B.D., Baumgartner, J.V., Powell, J., Braun, D.P., 1996. A method for assessing hydrologic alteration within ecosystems. Conserv. Biol. 10, 1163–1174.

Richter, B.D., Baumgartner, J.V., Wigington, R., Braun, D.P., 1997. How much water does a river need? Freshw. Biol. 37, 231–249.

Sahoo, G.B., Ray, C., De Carlo, E.H., 2006. Calibration and validation of a physically distributed hydrological model, MIKE SHE, to predict streamflow at high frequency in a flashy mountainous Hawaii stream. J. Hydrol. 327, 94–109.

Shopea, N., 2003. Station Profiles of Water Quality Monitoring Network in Cambodia: MRC Water Quality Monitoring Station Network Review. Mekong River Commission, Phnom Penh.

Singh, C.R., Thompson, J.R., French, J.R., Kingston, D.G., Mackay, A.W., 2010. Modelling the impact of prescribed global warming on runoff from headwater catchments of the Irrawaddy River and their implications for the water level regime of Loktak Lake, northeast India. Hydrol. Earth Syst. Sci. 14, 1745–1765.

Singh, C.R., Thompson, J.R., Kingston, D.G., French, J.R., 2011. Modelling water-level options for ecosystem services and assessment of climate change: Loktak Lake, northeast India. Hydrol. Sci. J. 56, 1518-1542.

Stisen, S., Jensen, K.H., Sandholt, I., Grimes, D.I.F., 2008. A remote sensing driven distributed hydrological model of the Senegal River basin. J. Hydrol. 354, 131–148.

Stone, R. 2010. Along with power, questions flow at Laos's new dam. Science 328, 414-415.

Takeuchi, K., 2008. Studies on the Mekong River Basin–modelling of hydrology and water resources. Hydrol. Process. 22, 1243–1245.

Thompson, J.R., 2012. Modelling the impacts of climate change on upland catchments in southwest Scotland using MIKE SHE and the UKCP09 probabilistic projections. Hydrol. Res. 43, 507–530.

Thompson, J.R., Refstrup Sørenson, H., Gavin, H., Refsgaard A., 2004. Application of the coupled MIKE SHE / MIKE 11 modelling system to a lowland wet grassland in Southeast England. J. Hydrol. 293, 151–179.

Thompson, J.R., Gavin, H., Refsgaard, A., Refstrup Sørenson, H., Gowing, D.J., 2009. Modelling the hydrological impacts of climate change on UK lowland wet grassland. Wetl. Ecol. Manag. 17, 503–523.

Todd, M.C., Taylor, R.G., Osborn, T., Kingston, D., Arnell, N., Gosling, S., 2011. Uncertainty in climate change impacts on basin-scale freshwater resources – preface to the special issue: the QUEST-GSI methodology and synthesis of results. Hydrol. Earth Syst. Sci. 15, 1035-1046.

Västilä, K., Kummu, M., Sangmanee, C., Chinvanno, S., 2010. Modelling climate change impacts on the flood pulse in the Lower Mekong floodplains. J. Water Clim. Change 1, 67-86.

Vázquez, R.F., Feyen, L., Feyen, J., Refsgaard, J.C., 2002. Effect of grid size on effective parameters and model performance of the MIKE SHE code. Hydrol. Process. 16, 355–372.

Vieux, B.E., 2004. Distributed Hydrologic Modeling Using GIS. Kluwer Academic, Dordrecht.

Waliser, D.E., Jin, K., Kang, I.S., Stern, W.F., Schubert, S.D., Wu, M.L.C., Lau, K.M., Lee, M.I., Krishnamurthy, V., Kitoh, A., Meehl, G.A., Galin, V.Y., Satyan, V., Mandke, S.K., Wu, G., Liu, Y., Park, C.K., 2003. AGCM simulations of intra-seasonal variability associated with the Asian summer monsoon. Clim. Dyn. 21, 423–446.

Wang, B., Kang, I.S., Lee, J.Y., 2004. Ensemble simulation of Asian–Australian monsoon variability by 11 AGCMs. J. Clim. 17, 699–710.

Wang, J.J., Lu, X.X., Kummu, M., 2011. Sediment load estimates and variations in the lower Mekong River. River Res. Appl. 27, 33–46.

Xie, P., Arkin, P.A., 1997. Global precipitation: a 17-year monthly analysis based on gauge observations, satellite estimates and numerical model outputs. Bull. Am. Meteorol. Soc. 78, 2539–2558.

Xu, H., Taylor, R.G., Kingston, D.G., Jiang, T., Thompson, J.R., Todd, M., 2010. Hydrological modelling of the River Xiangxi using SWAT2005: a comparison of model parameterizations using station and gridded meteorological observations. Quat. Int. 226, 54-59.

Yan, J., Smith, K., 1994. Simulation of integrated surface water and ground water systems – Model formulation. Water Resour. Bull. 30, 1–12.

Tables

Table 1. Summary of key attributes of the MIKE SHE, SLURP and Mac-PDM.09 hydrological models of the Mekong.

Attribute	MIKE SHE	SLURP	Mac-PDM.09
Model type	Distributed, physically based model, with conceptual linear reservoir saturated zone component	Semi-distributed vertical water balance model	Semi-distributed conceptual water balance global hydrological model
River routing	Kinematic routing (MIKE 11)	Muskingum	None
Time step	Variable – max. 48 hours	Daily	Daily
Meteorological inputs+	P, T, PET	P, T	P, T, W, SH, LW_{net}, SW
PET method	Linacre PET calculated externally	Linacre PET calculated within the model	Penman-Monteith PET calculated within the model
Snow scheme	Degree-day	Degree-day	Degree-day
Meteorological inputs spatial distribution	Distributed according to 13 sub-catchments from SLURP (Figure 1)	Distributed according to 13 sub-catchments (Figure 1)	0.5° × 0.5° grid
Spatial distribution of catchment characteristics	Topography, land cover and soil: based on 1 km × 1 km gridded data resampled to a 10 km × 10 km computational grid	Topography, land cover and soil: based on a 1 km × 1 km gridded data	Land cover and soil: 0.5° × 0.5° grid
Spatial resolution of process computation	All model components except the saturated zone: distributed according to 10 km × 10 km grid. Saturated zone: distributed according to 17 sub-catchments, each comprising three interflow and two baseflow reservoirs (Figure 1).	13 sub-catchments divided into elements for water balance calculations based on land cover, with 98 elements for the Mekong catchment. Results for each element aggregated based on relative cover within each sub-catchment.	0.5° × 0.5° grid
Calibration parameters*	k_i, k_p, k_b, DZ_{frac}, P_{lapse}, T_{lapse}, DD	RC, M, FC, U	Not calibrated for the Mekong (see text)

+ P: precipitation, T: air temperature, PET: potential evapotranspiration, W: wind speed, SH: specific humidity, LW_{net}: net longwave radiation flux, SW: shortwave radiation flux (downward)

* k_i: interflow time constants for saturated zone interflow reservoirs, k_p: percolation time constants for saturated zone interflow reservoirs, k_b: time constants for baseflow reservoirs, DZ_{frac}: dead storage in the baseflow reservoirs, P_{lapse}: precipitation lapse rate, T_{lapse}: temperature lapse rate, DD: snow melt degree-day coefficient, RC: retention constants and capacities of the fast and slow soil stores, M: Manning's n roughness coefficient for overland flow, FC: soil field capacity coefficients, U: wind factor used in computation of Linacre PET

Table 2. MIKE SHE model performance statistics for twelve gauging stations within the Mekong Basin for the calibration period (1961-1990 unless stated otherwise). Letters after gauging station names refer to the labels used in Figure 1. Corresponding statistics from Kingston et al. (2011) for SLURP are shown in brackets for three stations. Model performance indicators are taken from Henriksen et al. (2008).

Station	Obs (m^3s^{-1})	Sim (m^3s^{-1})	Dv (%)+	NSE*	r#
Mekong at Chiang Saen (a)	2711.3	2735.3	+0.88 ☆☆☆☆☆	0.888 ☆☆☆☆☆	0.943
		(2921.1)	(+8.20) (☆☆☆☆)	(0.78) (☆☆☆☆)	
Mekong at Luang Prabang (b)	3980.2	4132.4	+3.82 ☆☆☆☆☆	0.892 ☆☆☆☆☆	0.947
Mekong at Vientiane (c)	4521.1	4740.9	+4.86 ☆☆☆☆☆	0.900 ☆☆☆☆☆	0.951
Mekong at Nakhon Phanom (d)	7031.6	7322.7	+4.14 ☆☆☆☆☆	0.910 ☆☆☆☆☆	0.955
Mekong at Mukdahan (e)	7602.4	7874.4	+3.58 ☆☆☆☆☆	0.907 ☆☆☆☆☆	0.953
Mekong at Pakse (f)	9836.8	10144.8	+3.13 ☆☆☆☆☆	0.901 ☆☆☆☆☆	0.951
		(9876.7)	(+0.90) (☆☆☆☆☆)	(0.890) (☆☆☆☆☆)	
Mekong at Stung Treng (1961–1969) (g)	13381.0	13911.8	+3.97 ☆☆☆☆☆	0.924 ☆☆☆☆☆	0.963
Mekong at Kratie (h)	13418.9	13579.8	+1.20 ☆☆☆☆☆	0.901 ☆☆☆☆☆	0.950
Mekong at Kompong Cham (1964–Mar 1974) (i)	13409.5	14237.8	+6.18 ☆☆☆☆	0.904 ☆☆☆☆☆	0.954
Mekong at Phnom Penh (1961–Mar 1974) (j)	13022.3	14719.4	+13.03 ☆☆☆	0.866 ☆☆☆☆☆	0.951
Chi at Yasothon (k)	202.3	204.1	+0.88 ☆☆☆☆☆	0.494 ☆☆	0.712
Mun at Ubon (l)	636.3	638.4	+0.34 ☆☆☆☆☆	0.550 ☆☆☆	0.750
		(899.5)	(+41.90) (☆)	(0.44) (☆☆)	

Performance indicator	Excellent ☆☆☆☆☆	Very good ☆☆☆☆	Fair ☆☆☆	Poor ☆☆	Very poor ☆
Dv	< 5%	5–10 %	10–20 %	20–40%	>40 %
NSE	>0.85	0.65–0.85	0.50–0.65	0.20–0.50	<0.20

+ percentage deviation in simulated mean flow from observed mean flow (Henriksen *et al.*, 2003), * Nash-Sutcliffe coefficient (Nash and Sutcliffe, 1970), # Pearson correlation coefficient

Table 3. MIKE SHE model performance statistics for ten gauging stations within the Mekong catchment for the validation period (1991-1998 unless stated otherwise). Letters after gauging station names refer to the labels used in Figure 1. Corresponding statistics from Kingston et al. (2011) for SLURP are shown in brackets for two stations. Model performance indicators are taken from Henriksen et al. (2008).

Station	Obs (m^3s^{-1})	Sim (m^3s^{-1})	Dv (%)+	NSE*	r#
Mekong at Chiang Saen (1991–Jun 1997) (a)	2490.3	2258.7	-9.30 ☆☆☆☆	0.813 ☆☆☆☆	0.850
		(2550.0)	(+2.40) (☆☆☆☆☆	(0.810) (☆☆☆☆)	
Mekong at Luang Prabang (1991–1997) (b)	3749.7	3448.9	-8.02 ☆☆☆☆	0.887 ☆☆☆☆☆	0.904
Mekong at Vientiane (1991–1996) (c)	4241.7	3969.1	-6.43 ☆☆☆☆	0.901 ☆☆☆☆☆	0.922
Mekong at Nakhon Phanom (1991–Nov 1995) (d)	7063.2	6404.3	-9.33 ☆☆☆☆	0.791 ☆☆☆☆	0.853
Mekong at Mukdahan (1991–1995) (e)	7434.4	6866.9	-7.63 ☆☆☆☆	0.812 ☆☆☆☆	0.853
Mekong at Pakse (1991–1998) (f)	9168.4	8400.5	-8.38 ☆☆☆☆	0.858 ☆☆☆☆☆	0.877
		(8783.4)	(-4.20) (☆☆☆☆☆	(0.770) (☆☆☆☆)	
Mekong at Stung Treng (1991–1993) (g)	12569.5	11139.8	-11.37 ☆☆☆	0.508 ☆☆☆	0.536
Mekong at Kratie (1991–1998) (h)	12505.7	11700.8	-6.44 ☆☆☆☆	0.734 ☆☆☆☆	0.759
Chi at Yasothon (1991–1995) (k)	200.4	166.8	-16.73 ☆☆☆	0.581 ☆☆☆	0.650
Mun at Ubon (1991–1993) (l)	486.8	440.0	-9.60 ☆☆☆☆	0.820 ☆☆☆☆	0.847

Performance indicator	Excellent ☆☆☆☆☆	Very good ☆☆☆☆	Fair ☆☆☆	Poor ☆☆	Very poor ☆
Dv	< 5%	5–10 %	10–20 %	20–40%	>40 %
NSE	>0.85	0.65–0.85	0.50–0.65	0.20–0.50	<0.20

+ percentage deviation in simulated mean flow from observed mean flow (Henriksen *et al.*, 2003), * Nash-Sutcliffe coefficient (Nash and Sutcliffe, 1970), # Pearson correlation coefficient

Table 4. Mean annual precipitation and potential evapotranspiration (PET) for the baseline (mm) and changes (%) for the climate change scenarios for representative sub-catchments within the Mekong catchment. (Numbers in brackets refer to the meteorological inputs sub-catchments identified in Figure 1. Shaded cells indicate negative changes compared to the baseline).

Parameter	Scenario	Lancang (1)	Mek. 1 (4)	Chi (5)	Mun (6)	Mek. 2 (8)	Se Kong (9)	Sre Pok (10)	Mek. 3 (11)
Precipitation	Baseline	1052.8	1855.8	1272.3	1313.6	2213.2	2432.5	2055.3	1870.3
	CCCMA	10.1	10.2	12.3	10.2	8.4	5.2	1.9	5.3
	CSIRO	-4.6	-4.6	-3.3	-2.9	-2.8	-2.8	-2.9	-1.3
	HadCM3	10.1	1.0	-0.1	-0.4	-1.1	-2.1	-4.5	-3.0
	HadGEM1	5.9	-3.7	-6.1	-4.8	-1.2	2.9	3.9	1.0
	IPSL	-5.2	-1.1	-0.1	-0.1	0.6	-0.4	1.3	-0.4
	MPI	3.6	7.0	10.2	10.3	8.8	6.6	7.6	12.2
	NCAR	8.5	9.1	5.0	3.5	1.9	3.5	3.7	5.3
PET	Baseline	1765.6	1923.0	2363.6	2336.5	1813.0	1728.5	1695.9	1770.3
	CCCMA	11.7	12.3	13.1	12.7	12.5	12.7	12.3	12.5
	CSIRO	14.6	15.7	15.9	15.2	15.2	14.9	14.2	14.3
	HadCM3	12.9	13.9	13.3	13.2	14.7	14.8	14.8	15.1
	HadGEM1	12.4	12.1	10.3	10.3	12.4	13.0	12.7	12.5
	IPSL	15.9	15.7	15.3	14.2	14.3	13.9	12.8	13.2
	MPI	13.6	13.6	13.3	12.9	13.4	13.5	13.1	13.2
	NCAR	11.3	10.9	11.1	10.6	11.4	11.1	10.7	10.3
Precipitation	Baseline	1052.8	1855.8	1272.3	1313.6	2213.2	2432.5	2055.3	1870.3
	1°C	5.0	0.4	-0.1	-0.3	-0.6	-1.3	-2.7	-1.7
	2°C	10.1	1.0	-0.1	-0.4	-1.1	-2.1	-4.5	-3.0
	3°C	15.2	1.6	0.1	-0.4	-1.3	-2.6	-5.6	-4.2
	4°C	20.2	2.4	0.4	-0.2	-1.3	-3.0	-6.3	-5.1
	5°C	25.3	3.3	0.9	0.1	-1.3	-3.1	-6.7	-6.0
	6°C	30.2	4.3	1.5	0.5	-1.1	-3.2	-6.9	-6.7
PET	Baseline	1765.6	1923.0	2363.6	2336.5	1813.0	1728.5	1695.9	1770.3
	1°C	6.3	6.8	6.4	6.2	7.3	7.4	7.3	7.2
	2°C	12.9	13.9	13.3	13.2	14.7	14.8	14.8	15.1
	3°C	19.8	21.3	20.6	20.6	22.4	22.5	22.6	23.5
	4°C	26.9	29.1	28.2	28.3	30.5	30.5	30.8	32.2
	5°C	34.4	37.3	36.3	36.5	39.0	39.0	39.3	41.4
	6°C	42.2	45.9	44.8	45.1	47.9	47.8	48.3	51.1

Table 5. Mean, Q5 and Q95 discharges (m^3s^{-1}) simulated by MIKE SHE for the baseline and changes (%) for the 2 °C, seven GCM scenarios at eight gauging stations within the Mekong catchment. (Letters in brackets refer to the gauging station labels used in Figure 1. Shaded cells indicate negative changes compared to the baseline).

Discharge	Scenario	Chiang Saen (a)	Luang Prabang (b)	Vientiane (c)	Mukdahan (e)	Pakse (f)	Kratie (h)	Phnom Penh (j)	Ubon (l)
Mean	Baseline	2735.3	4132.4	4740.9	7874.4	10144.8	13579.8	13942.4	638.4
	CCCMA	7.3	6.9	7.4	8.3	9.0	7.2	7.0	11.0
	CSIRO	-21.2	-21.6	-21.1	-17.7	-16.4	-14.7	-14.4	-11.4
	HadCM3	11.3	9.9	7.8	3.7	1.4	-1.7	-2.1	-8.2
	HadGEM1	0.2	-3.5	-5.6	-8.5	-10.4	-9.1	-9.0	-20.6
	IPSL	-19.7	-18.1	-16.8	-12.6	-10.6	-9.4	-9.4	-3.0
	MPI	-2.3	-1.0	0.2	2.6	4.9	5.6	5.9	16.5
	NCAR	8.7	12.4	12.6	12.7	11.2	8.2	8.0	2.9
Q5	Baseline	6920.5	10523.9	12135.5	21635.8	28188.2	38302.0	39560.1	2037.3
	CCCMA	-3.5	0.2	-1.1	8.1	10.2	7.4	8.0	18.6
	CSIRO	-19.6	-19.0	-16.4	-13.5	-12.8	-10.9	-11.0	-1.9
	HadCM3	4.9	4.0	3.5	-1.4	-2.5	-4.9	-5.3	-3.7
	HadGEM1	-4.8	-6.8	-6.8	-11.8	-14.9	-15.6	-14.8	-11.9
	IPSL	-13.7	-7.8	-10.2	-6.5	-1.6	-3.3	-3.8	10.1
	MPI	-4.8	1.3	1.0	2.9	6.1	6.5	6.5	19.3
	NCAR	6.5	11.0	9.2	12.3	7.7	6.8	6.2	11.6
Q95	Baseline	767.9	1092.6	1234.0	1345.2	1438.4	1560.9	1583.1	23.9
	CCCMA	7.5	13.0	13.4	13.5	16.3	14.3	13.1	22.0
	CSIRO	-23.2	-23.5	-21.4	-18.2	-17.7	-18.2	-19.1	-15.0
	HadCM3	12.9	11.0	9.0	11.4	9.2	9.0	8.2	-6.3
	HadGEM1	-1.6	-2.6	-2.9	-4.4	-4.1	-3.9	-4.7	-17.5
	IPSL	-21.9	-18.3	-16.9	-16.4	-15.7	-15.9	-16.2	-9.4
	MPI	-3.2	-0.6	-0.8	-0.6	0.3	-0.2	-1.3	6.8
	NCAR	11.4	17.0	17.7	20.3	19.5	17.7	16.6	3.2

Table 6. Mean, Q5 and Q95 discharges (m^3s^{-1}) simulated by MIKE SHE for the baseline and changes (%) for the 1-6 °C, HadCM3 scenarios at eight gauging stations within the Mekong catchment. (Letters in brackets refer to the gauging station labels used in Figure 1. Shaded cells indicate negative changes compared to the baseline).

Discharge	Scenario	Chiang Saen (a)	Luang Prabang (b)	Vientiane (c)	Mukdahan (e)	Pakse (f)	Kratie (h)	Phnom Penh (j)	Ubon (l)
Mean	Baseline	2735.3	4132.4	4740.9	7874.4	10144.8	13579.8	13942.4	638.4
	1°C	6.5	5.5	4.5	2.2	1.0	-0.7	-0.9	-5.1
	2°C	11.3	9.9	7.8	3.7	1.4	-1.7	-2.1	-8.2
	3°C	14.1	12.3	9.4	4.0	0.9	-3.1	-3.6	-14.1
	4°C	18.1	16.4	12.5	5.4	1.5	-3.6	-4.2	-14.9
	5°C	22.5	20.5	15.7	7.1	2.0	-4.2	-5.1	-21.6
	6°C	28.7	25.5	19.6	8.9	3.0	-4.3	-5.3	-24.2
Q5	Baseline	6920.5	10523.9	12135.5	21635.8	28188.2	38302.0	39560.1	2037.3
	1°C	-1.1	1.3	-0.2	-1.4	-1.1	-3.8	-3.2	1.1
	2°C	4.9	4.0	3.5	-1.4	-2.5	-4.9	-5.3	-3.7
	3°C	6.0	6.7	3.0	-2.6	-2.2	-7.4	-8.0	-8.7
	4°C	9.9	10.8	6.5	-3.4	-5.7	-7.6	-8.0	-9.7
	5°C	16.1	14.7	7.3	1.6	-4.8	-7.5	-9.3	-10.4
	6°C	21.3	20.2	12.1	1.0	-2.8	-7.5	-8.8	-11.0
Q95	Baseline	767.9	1092.6	1234.0	1345.2	1438.4	1560.9	1583.1	23.9
	1°C	4.6	6.8	6.5	5.8	5.1	4.3	3.4	-6.3
	2°C	12.9	11.0	9.0	11.4	9.2	9.0	8.2	-6.3
	3°C	18.6	19.2	14.6	14.3	14.7	10.4	9.2	-15.8
	4°C	22.6	21.1	17.9	15.4	14.3	10.0	8.9	-22.0
	5°C	27.1	28.8	21.7	17.3	14.1	9.7	8.8	-31.8
	6°C	37.3	33.6	29.0	24.1	22.1	16.6	15.0	-38.4

Figure Captions

Figure 1. The Mekong catchment and its representation within the MIKE SHE model including the distribution of linear reservoir sub-catchments, interflow reservoirs and meteorological inputs. The gauging stations within the MIKE 11 river network that were used for calibration and validation are also indicated.

Figure 2. Monthly mean observed and MIKE SHE simulated discharge for five gauging station along the Mekong River for the calibration period (1961–1990). (Letters in brackets refer to the gauging station labels used in Figure 1).

Figure 3. Observed and MIKE SHE simulated river regimes for all 12 gauging stations within the Mekong catchment for the calibration period (1961-1990 unless indicated otherwise). Regimes simulated by SLURP for three gauging stations are also shown. (Letters in brackets refer to the gauging station labels used in Figure 1).

Figure 4. Mean monthly precipitation and PET for the baseline and the 2 °C, seven GCM climate change scenarios for four representative sub-catchments. (Note different y-axis scales. Numbers in brackets refer to the meteorological inputs sub-catchments identified in Figure 1).

Figure 5. River regimes simulated by MIKE SHE for the baseline and 2 °C, seven GCM climate change scenarios for eight gauging stations within the Mekong catchment. (Letters in brackets refer to the gauging station labels used in Figure 1).

Figure 6. Percentage change in mean annual discharge simulated by MIKE SHE for four gauging stations within the Mekong catchment resulting from combined and individual modifications to

precipitation, PET and temperature for the 2 °C, seven GCM climate change scenarios. (Note the different y-axis scales. Letters in brackets refer to the gauging station labels used in Figure 1).

Figure 7. Change from baseline mean annual discharge (runoff for Mac-PDM.09) for the 2 °C, seven GCM climate change scenarios for six gauging stations within the Mekong catchment, as simulated by the three hydrological models. (CC: CCCMA; CS: CSIRO; H3: HadCM3; H1: HadGEM1; I: IPSL; M: MPI; N: NCAR. Letters in brackets refer to the gauging station labels used in Figure 1).

Figure 8. Mean monthly discharge (runoff for Mac-PDM.09) as a percentage of the mean annual total for the 2 °C, seven GCM climate change scenarios for five gauging stations, as simulated by the three hydrological models. (Letters in brackets refer to the gauging station labels used in Figure 1).

Figure 9. Mean monthly precipitation and PET for the baseline and 1–6 °C, HadCM3 climate change scenarios. (Note the different y-axis scales. Numbers in brackets refer to the meteorological inputs sub-catchments identified in Figure 1).

Figure 10. River regimes simulated by MIKE SHE for the baseline and 1–6 °C, HadCM3 climate change scenarios for eight gauging stations within the Mekong catchment. (Letters in brackets refer to the gauging station labels used in Figure 1).

Figure 11. Percentage change in mean annual discharge simulated by MIKE SHE for four gauging stations within the Mekong catchment resulting from combined and individual modifications to precipitation, PET and temperature for the 1–6 °C, HadCM3 climate change scenarios. (Note the different y-axis scales. Letters in brackets refer to the gauging station labels used in Figure 1).

Figure 12. Change from baseline mean annual discharge (runoff for Mac-PDM.09) for the 1–6 °C, HadCM3 climate change scenarios for six gauging stations within the Mekong catchment, as simulated by the three hydrological model. (Letters in brackets refer to the gauging station labels used in Figure 1).

Figure 13. Mean monthly discharge (runoff for Mac-PDM.09) as a percentage of the mean annual total for the 1–6 °C, HadCM3 climate change scenarios for five gauging stations, as simulated by the three hydrological models. (Letters in brackets refer to the gauging station labels used in Figure 1).

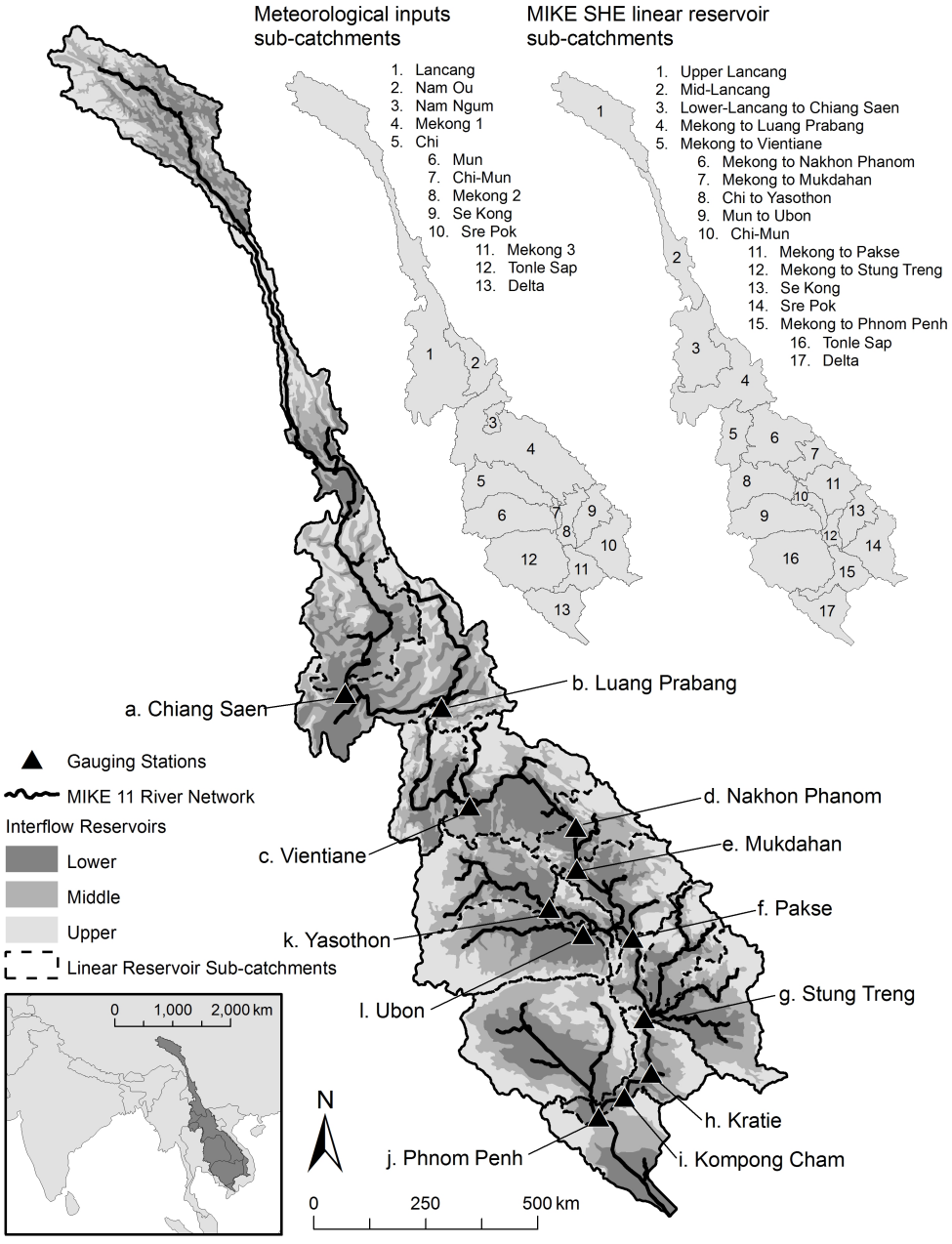
Meteorological inputs sub-catchments
1. Lancang
2. Nam Ou
3. Nam Ngum
4. Mekong 1
5. Chi
6. Mun
7. Chi-Mun
8. Mekong 2
9. Se Kong
10. Sre Pok
11. Mekong 3
12. Tonle Sap
13. Delta
MIKE SHE linear reservoir sub-catchments
1. Upper Lancang
2. Mid-Lancang
3. Lower-Lancang to Chiang Saen
4. Mekong to Luang Prabang
5. Mekong to Vientiane
6. Mekong to Nakhon Phanom
7. Mekong to Mukdahan
8. Chi to Yasothon
9. Mun to Ubon
10. Chi-Mun
11. Mekong to Pakse
12. Mekong to Stung Treng
13. Se Kong
14. Sre Pok
15. Mekong to Phnom Penh
16. Tonle Sap
17. Delta
a. Chiang Saen
b. Luang Prabang
c. Vientiane
d. Nakhon Phanom
e. Mukdahan
f. Pakse
g. Stung Treng
h. Kratie
i. Kompong Cham
j. Phnom Penh
k. Yasothon
l. Ubon
Gauging Stations
MIKE 11 River Network
Interflow Reservoirs
Lower
Middle
Upper
Linear Reservoir Sub-catchments
0 1,000 2,000 km
N
0 250 500 km

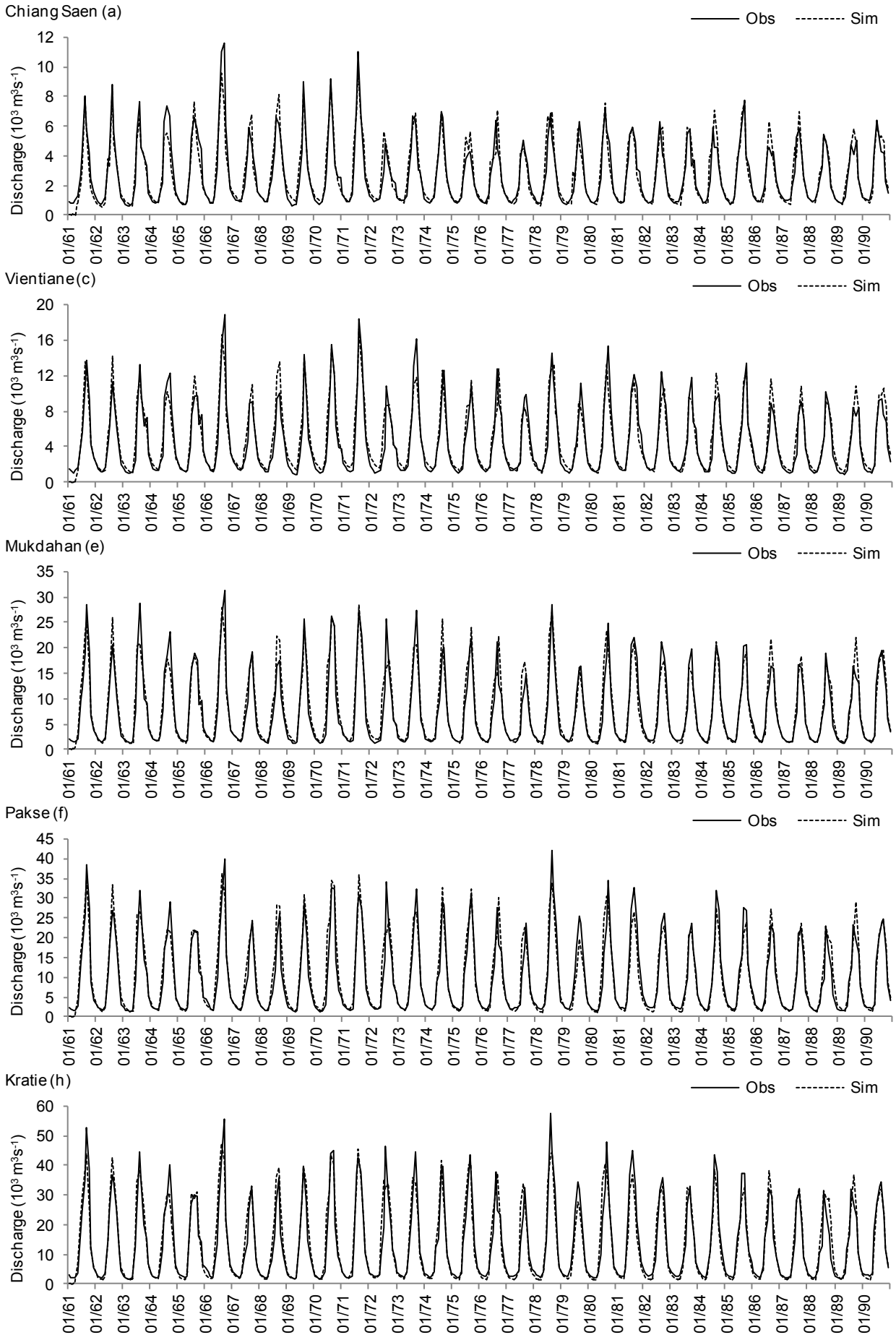
Chiang Saen (a)
Obs
Sim
Discharge (10^3 m^3s^{-1})
0
2
4
6
8
10
12
01/61
01/62
01/63
01/64
01/65
01/66
01/67
01/68
01/69
01/70
01/71
01/72
01/73
01/74
01/75
01/76
01/77
01/78
01/79
01/80
01/81
01/82
01/83
01/84
01/85
01/86
01/87
01/88
01/89
01/90
Vientiane (c)
Obs
Sim
Discharge (10^3 m^3s^{-1})
0
4
8
12
16
20
01/61
01/62
01/63
01/64
01/65
01/66
01/67
01/68
01/69
01/70
01/71
01/72
01/73
01/74
01/75
01/76
01/77
01/78
01/79
01/80
01/81
01/82
01/83
01/84
01/85
01/86
01/87
01/88
01/89
01/90
Mukdahan (e)
Obs
Sim
Discharge (10^3 m^3s^{-1})
0
5
10
15
20
25
30
35
01/61
01/62
01/63
01/64
01/65
01/66
01/67
01/68
01/69
01/70
01/71
01/72
01/73
01/74
01/75
01/76
01/77
01/78
01/79
01/80
01/81
01/82
01/83
01/84
01/85
01/86
01/87
01/88
01/89
01/90
Pakse (f)
Obs
Sim
Discharge (10^3 m^3s^{-1})
0
5
10
15
20
25
30
35
40
45
01/61
01/62
01/63
01/64
01/65
01/66
01/67
01/68
01/69
01/70
01/71
01/72
01/73
01/74
01/75
01/76
01/77
01/78
01/79
01/80
01/81
01/82
01/83
01/84
01/85
01/86
01/87
01/88
01/89
01/90
Kratie (h)
Obs
Sim
Discharge (10^3 m^3s^{-1})
0
10
20
30
40
50
60
01/61
01/62
01/63
01/64
01/65
01/66
01/67
01/68
01/69
01/70
01/71
01/72
01/73
01/74
01/75
01/76
01/77
01/78
01/79
01/80
01/81
01/82
01/83
01/84
01/85
01/86
01/87
01/88
01/89
01/90

Figure 2.

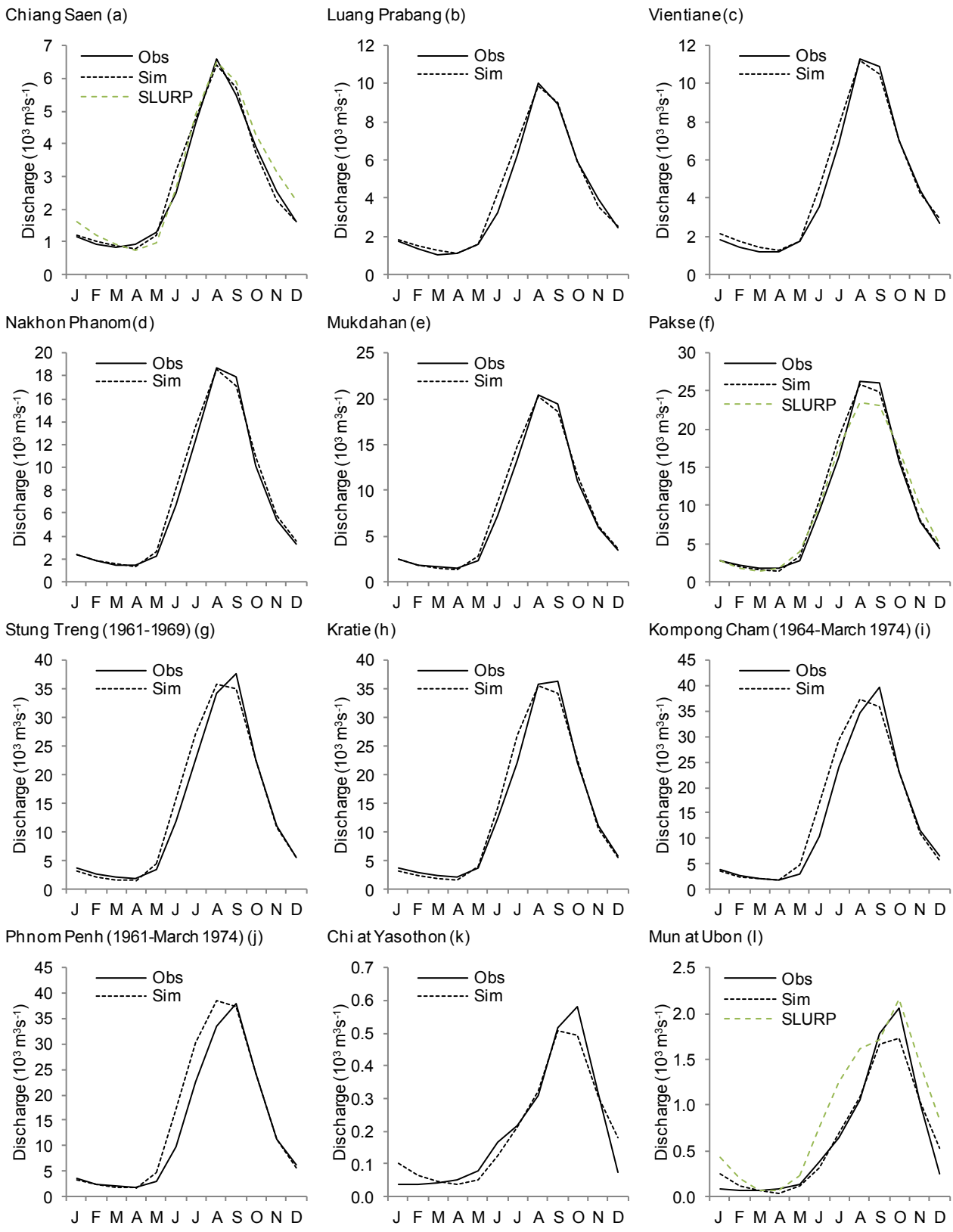
Chiang Saen (a)
Luang Prabang (b)
Vientiane (c)
Nakhon Phanom (d)
Mukdahan (e)
Pakse (f)
Stung Treng (1961-1969) (g)
Kratie (h)
Kompong Cham (1964-March 1974) (i)
Phnom Penh (1961-March 1974) (j)
Chi at Yasothon (k)
Mun at Ubon (l)
Obs
Sim
SLURP
Discharge (10³ m³s⁻¹)
J F M A M J J A S O N D

Figure 3.

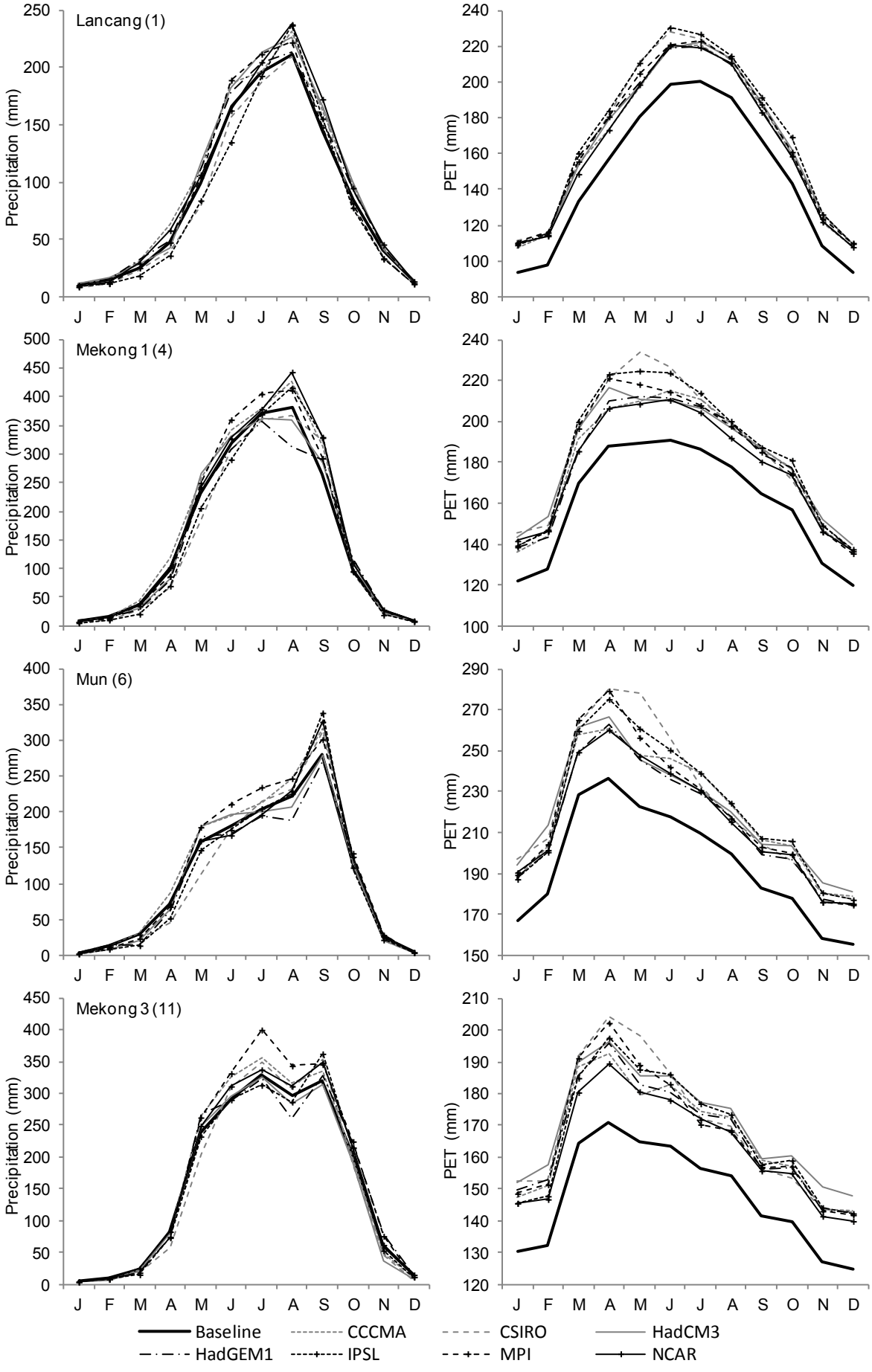
Lancang (1)
Mekong 1 (4)
Mun (6)
Mekong 3 (11)
Precipitation (mm)
PET (mm)
J F M A M J J A S O N D
Baseline
CCCMA
CSIRO
HadCM3
HadGEM1
IPSL
MPI
NCAR

Figure 4.

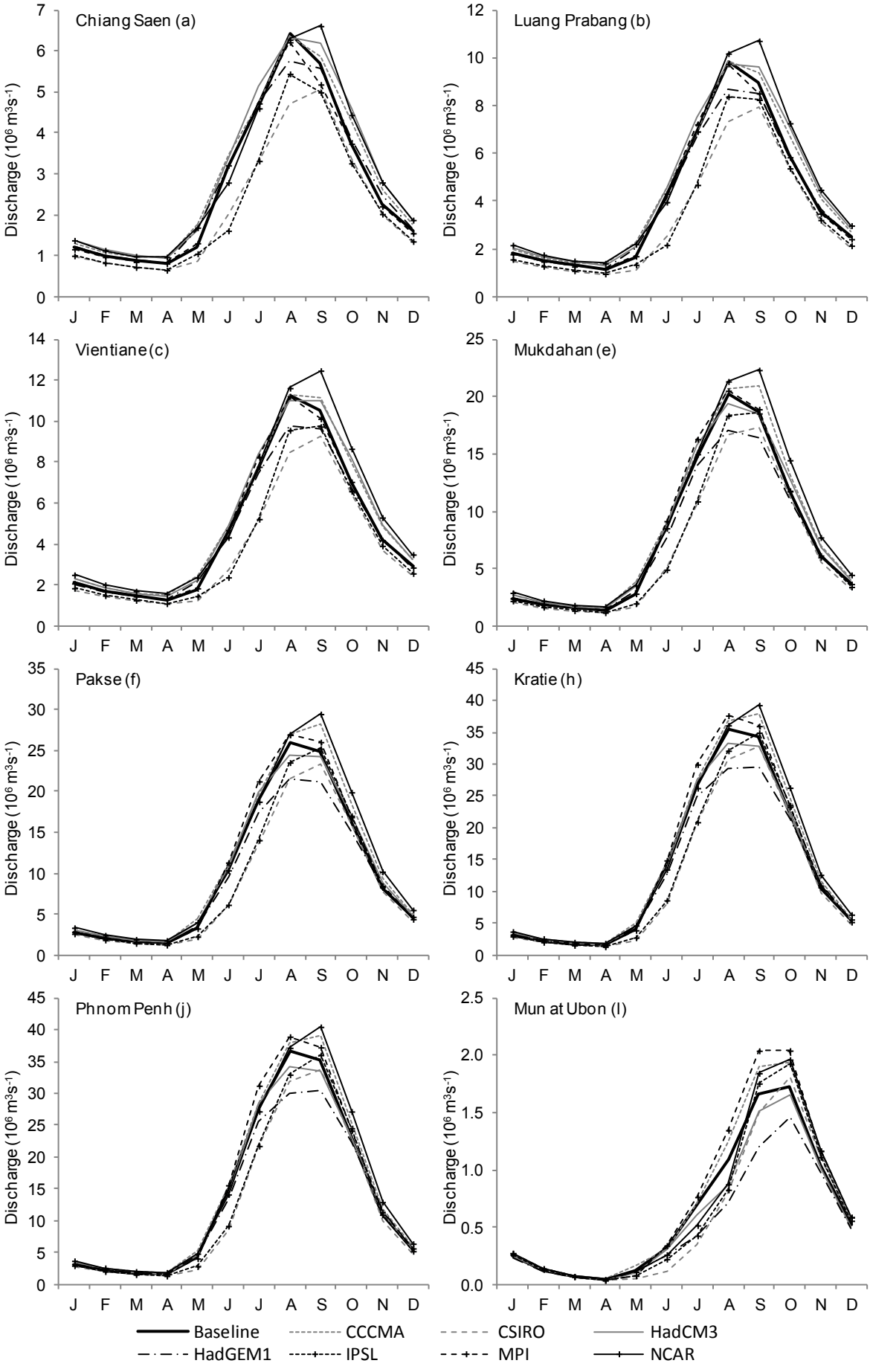
Chiang Saen (a)
Luang Prabang (b)
Vientiane (c)
Mukdahan (e)
Pakse (f)
Kratie (h)
Phnom Penh (j)
Mun at Ubon (l)
Discharge (10^6 m^3s^{-1})
J F M A M J J A S O N D
Baseline
CCCMA
CSIRO
HadCM3
HadGEM1
IPSL
MPI
NCAR

Figure 5.

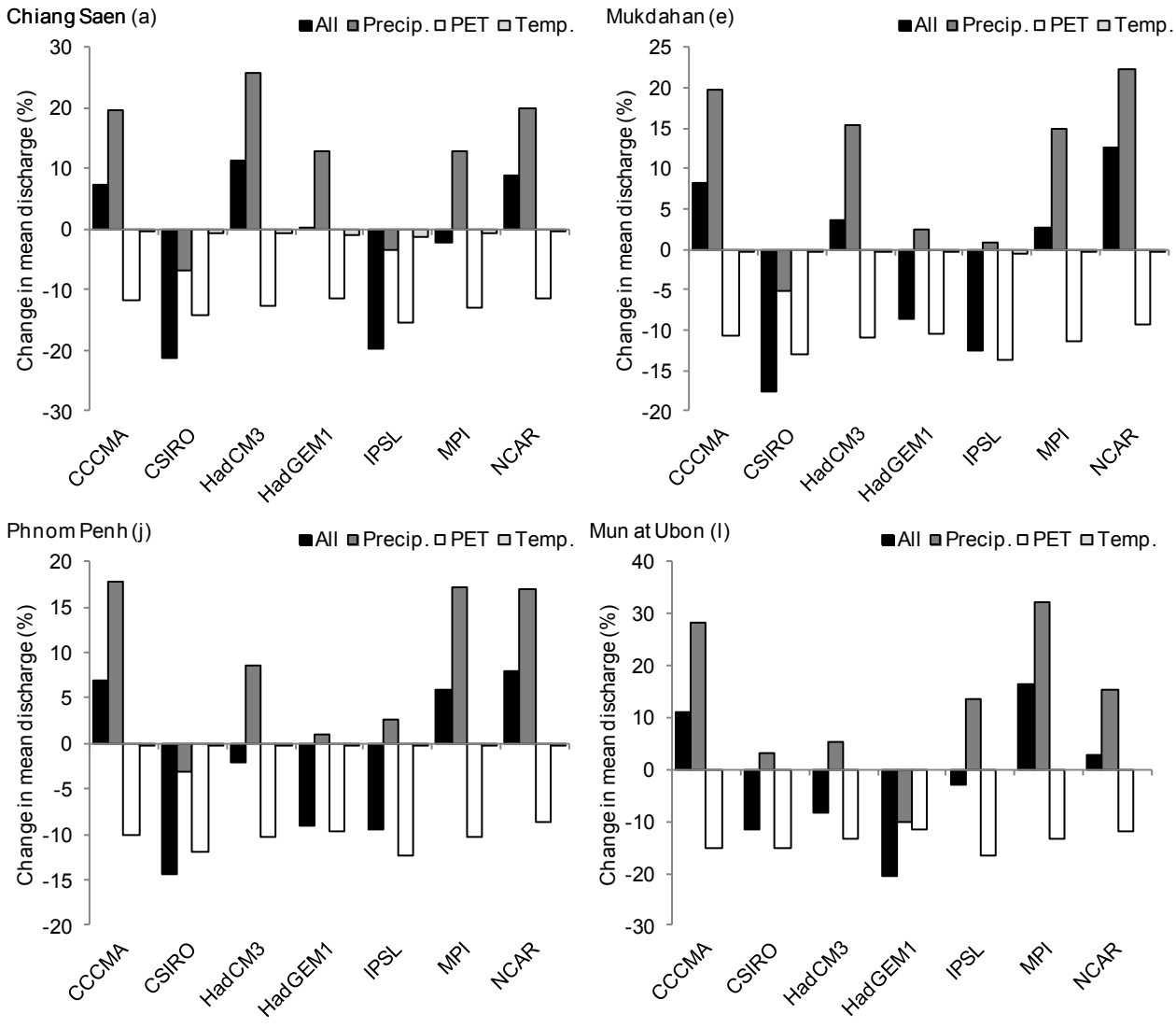
Chiang Saen (a)
All
Precip.
PET
Temp.
Change in mean discharge (%)
30
20
10
0
-10
-20
-30
CCCMA
CSIRO
HadCM3
HadGEM1
IPSL
MPI
NCAR
Mukdahan (e)
All
Precip.
PET
Temp.
Change in mean discharge (%)
25
20
15
10
5
0
-5
-10
-15
-20
CCCMA
CSIRO
HadCM3
HadGEM1
IPSL
MPI
NCAR
Phnom Penh (j)
All
Precip.
PET
Temp.
Change in mean discharge (%)
20
15
10
5
0
-5
-10
-15
-20
CCCMA
CSIRO
HadCM3
HadGEM1
IPSL
MPI
NCAR
Mun at Ubon (l)
All
Precip.
PET
Temp.
Change in mean discharge (%)
40
30
20
10
0
-10
-20
-30
CCCMA
CSIRO
HadCM3
HadGEM1
IPSL
MPI
NCAR

Figure 6.

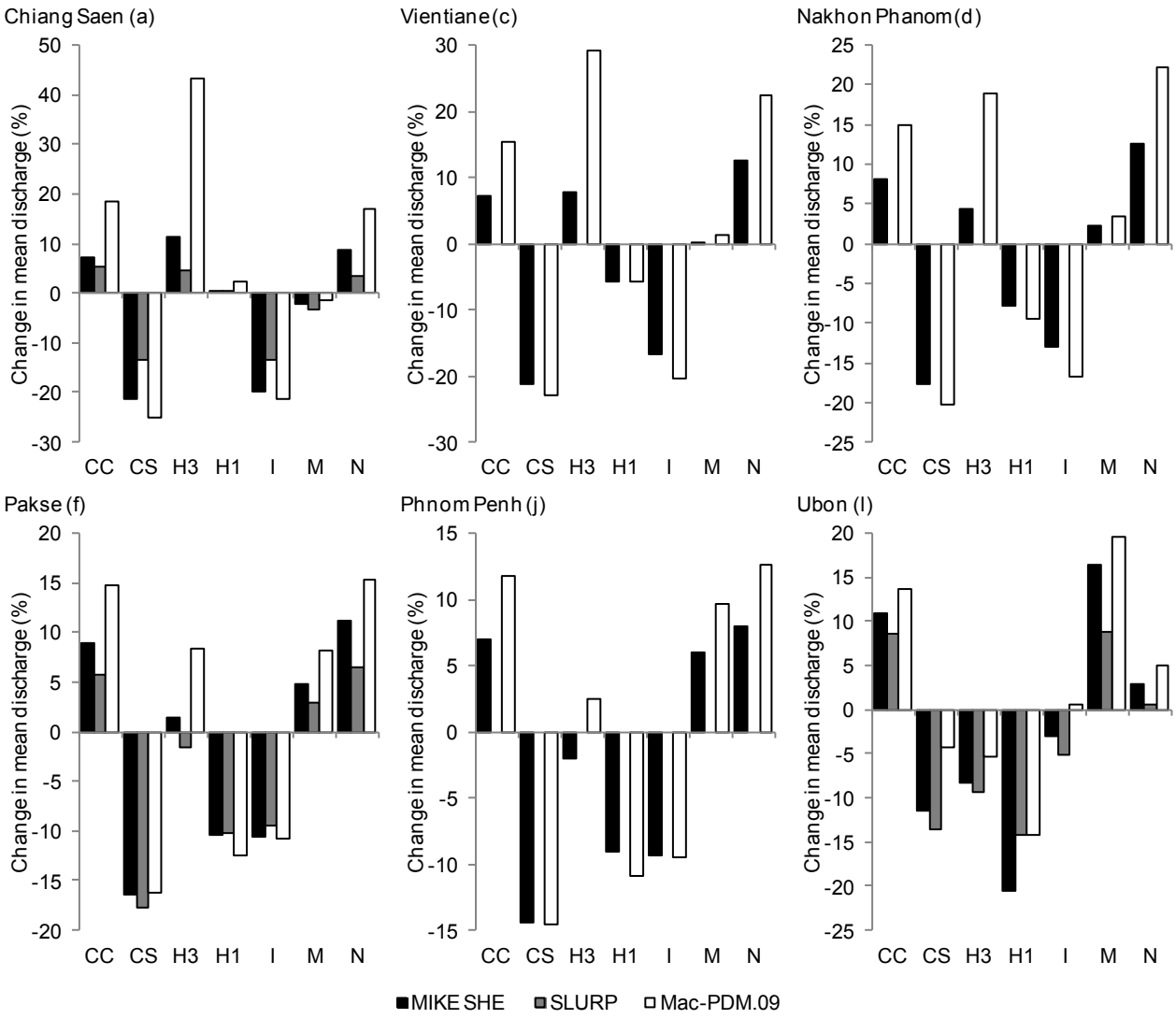
Chiang Saen (a)
Vientiane (c)
Nakhon Phanom (d)
Pakse (f)
Phnom Penh (j)
Ubon (l)
Change in mean discharge (%)
CC CS H3 H1 I M N
MIKE SHE
SLURP
Mac-PDM.09

Figure 7.

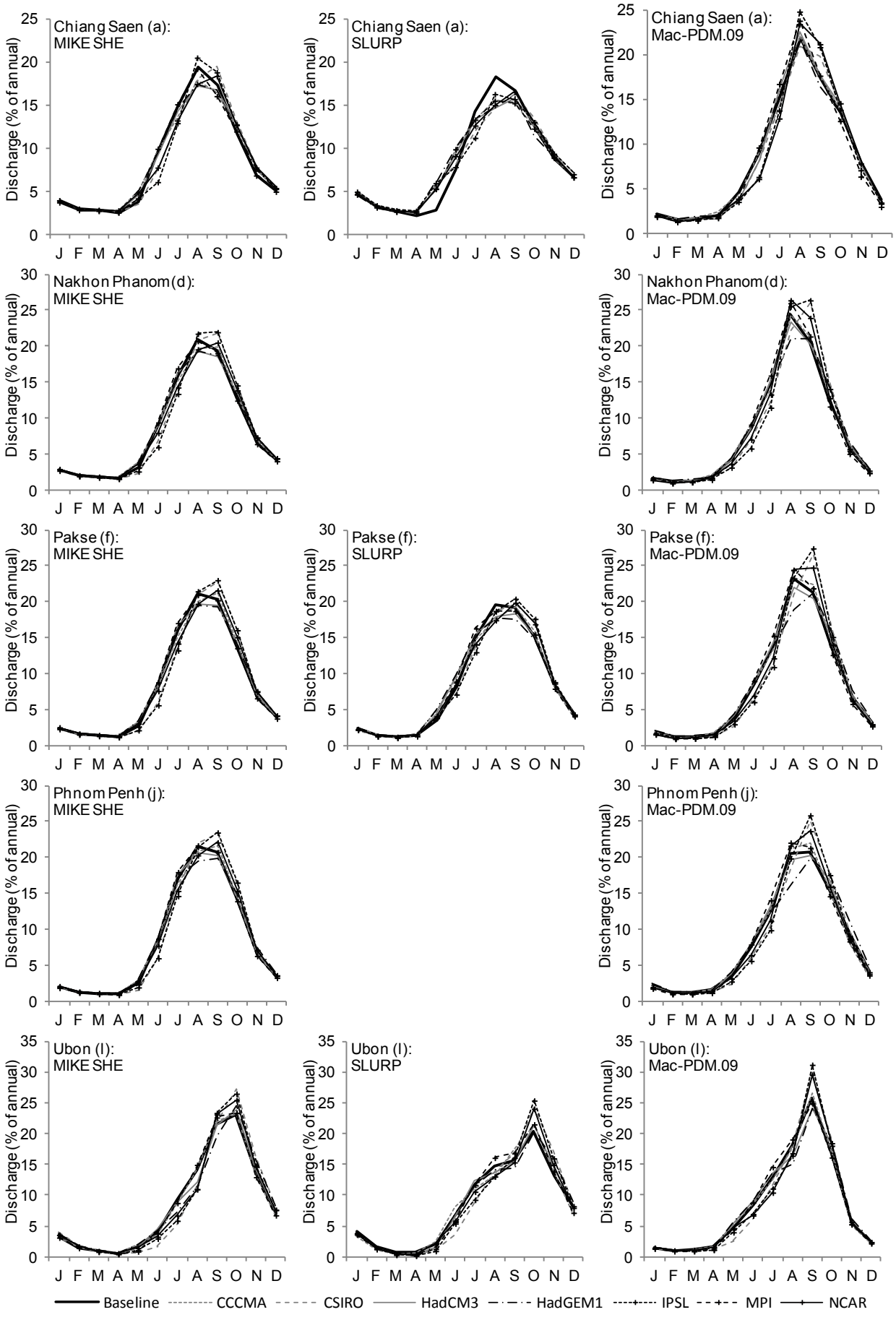
Chiang Saen (a): MIKE SHE
Chiang Saen (a): SLURP
Chiang Saen (a): Mac-PDM.09
Nakhon Phanom (d): MIKE SHE
Nakhon Phanom (d): Mac-PDM.09
Pakse (f): MIKE SHE
Pakse (f): SLURP
Pakse (f): Mac-PDM.09
Phnom Penh (j): MIKE SHE
Phnom Penh (j): Mac-PDM.09
Ubon (l): MIKE SHE
Ubon (l): SLURP
Ubon (l): Mac-PDM.09
Discharge (% of annual)
J F M A M J J A S O N D
Baseline
CCCMA
CSIRO
HadCM3
HadGEM1
IPSL
MPI
NCAR

Figure 8.

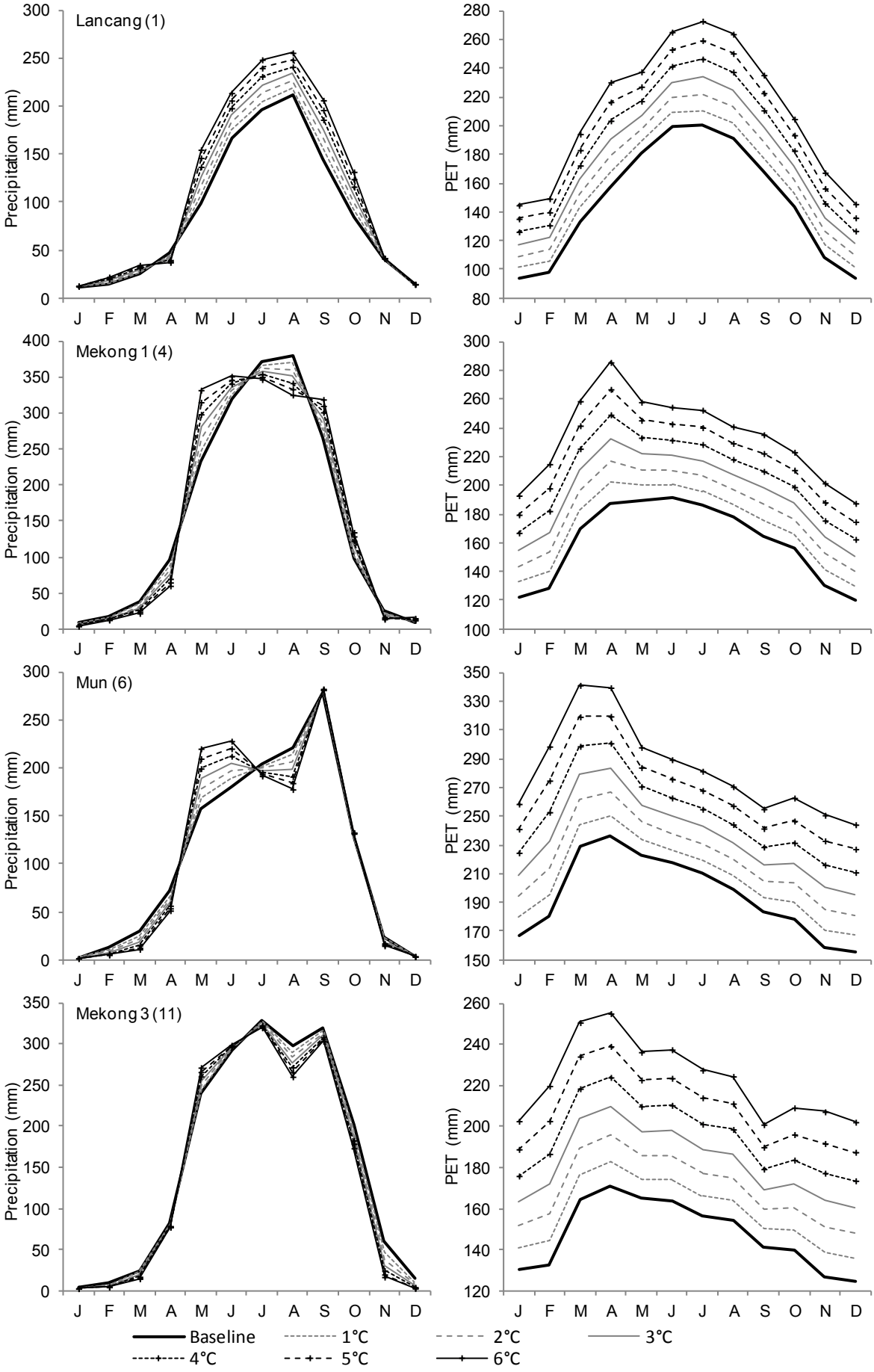
Lancang (1)
Mekong 1 (4)
Mun (6)
Mekong 3 (11)
Precipitation (mm)
PET (mm)
J F M A M J J A S O N D
Baseline
1°C
2°C
3°C
4°C
5°C
6°C

Figure 9.

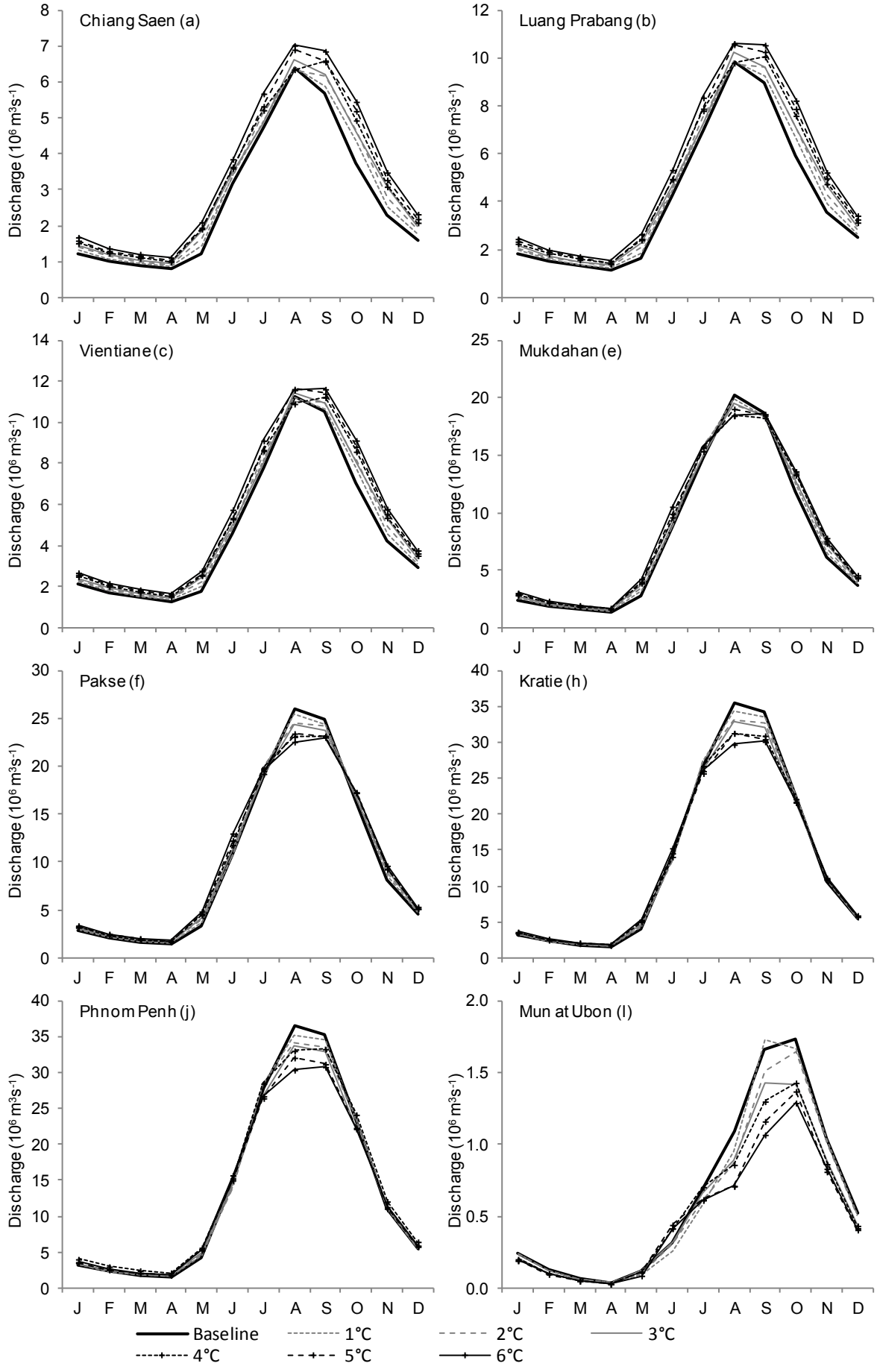
Chiang Saen (a)
Luang Prabang (b)
Vientiane (c)
Mukdahan (e)
Pakse (f)
Kratie (h)
Phnom Penh (j)
Mun at Ubon (l)
Discharge (10^6 m^3s^{-1})
J F M A M J J A S O N D
Baseline
1°C
2°C
3°C
4°C
5°C
6°C

Figure 10.

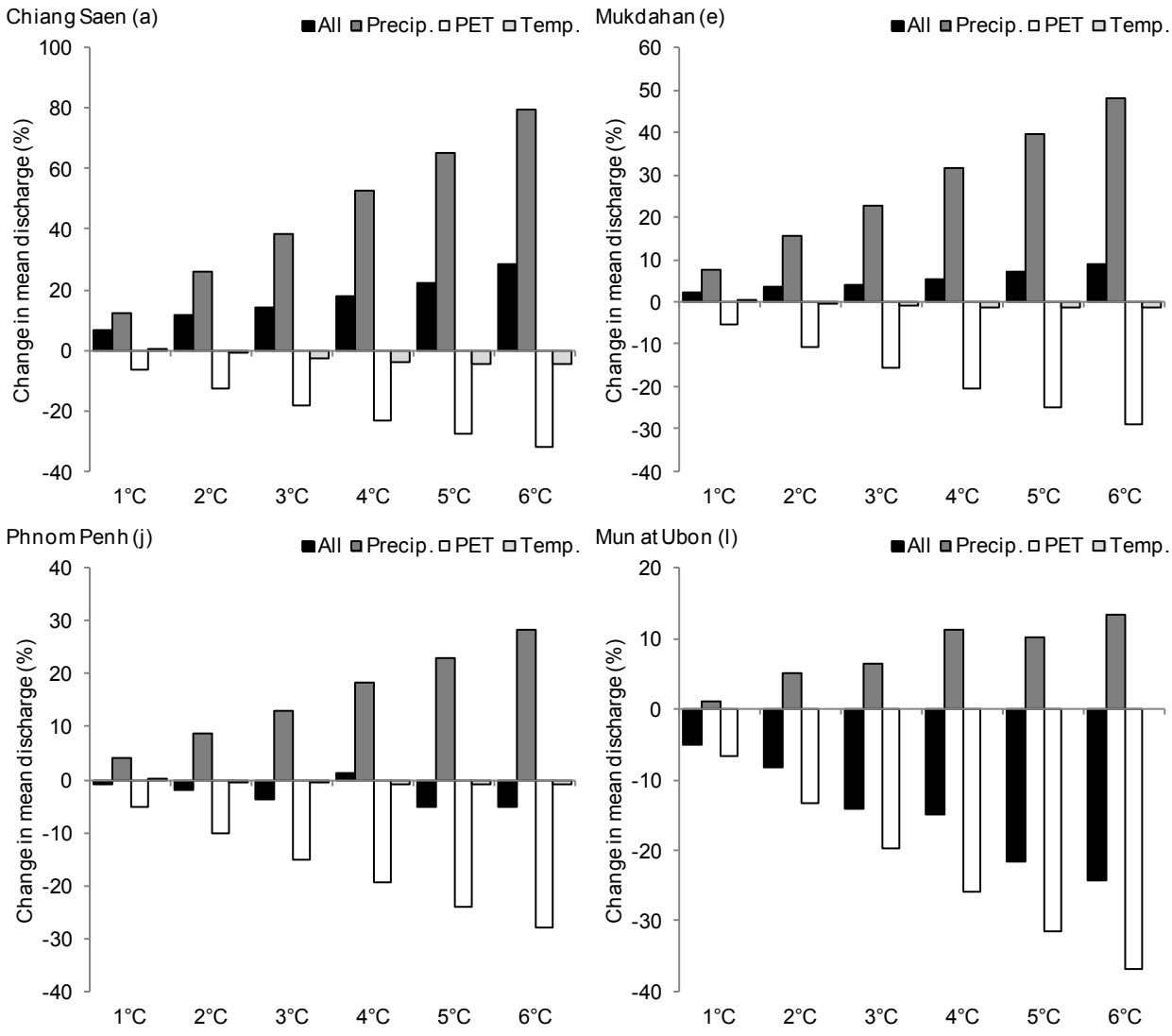
Chiang Saen (a)
All
Precip.
PET
Temp.
Change in mean discharge (%)
100
80
60
40
20
0
-20
-40
1°C
2°C
3°C
4°C
5°C
6°C
Mukdahan (e)
All
Precip.
PET
Temp.
Change in mean discharge (%)
60
50
40
30
20
10
0
-10
-20
-30
-40
1°C
2°C
3°C
4°C
5°C
6°C
Phnom Penh (j)
All
Precip.
PET
Temp.
Change in mean discharge (%)
40
30
20
10
0
-10
-20
-30
-40
1°C
2°C
3°C
4°C
5°C
6°C
Mun at Ubon (l)
All
Precip.
PET
Temp.
Change in mean discharge (%)
20
10
0
-10
-20
-30
-40
1°C
2°C
3°C
4°C
5°C
6°C

Figure 11.

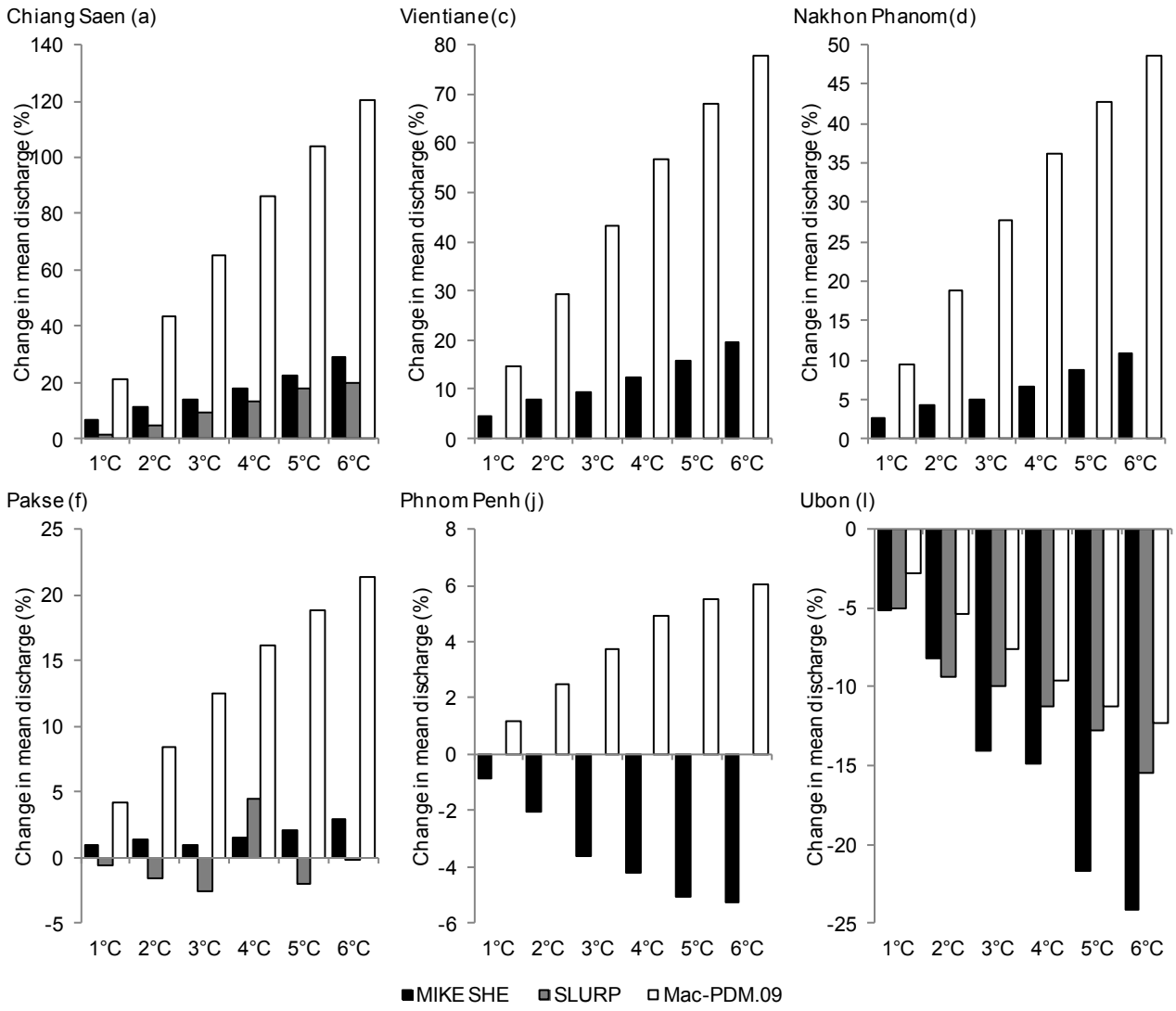
Chiang Saen (a)
Vientiane (c)
Nakhon Phanom (d)
Pakse (f)
Phnom Penh (j)
Ubon (l)
Change in mean discharge (%)
1°C 2°C 3°C 4°C 5°C 6°C
MIKE SHE
SLURP
Mac-PDM.09

Figure 12.

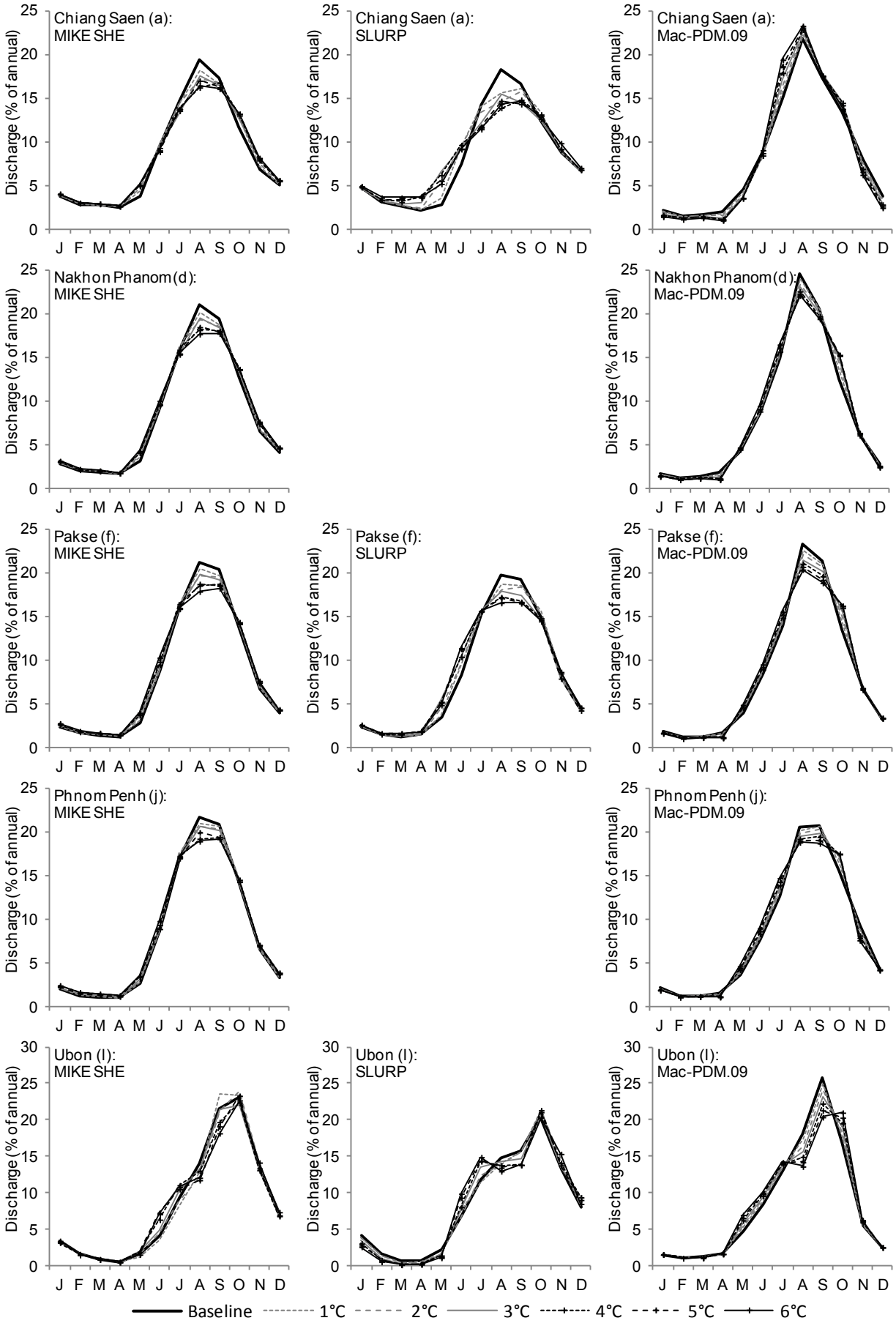
Chiang Saen (a): MIKE SHE
Chiang Saen (a): SLURP
Chiang Saen (a): Mac-PDM.09
Nakhon Phanom (d): MIKE SHE
Nakhon Phanom (d): Mac-PDM.09
Pakse (f): MIKE SHE
Pakse (f): SLURP
Pakse (f): Mac-PDM.09
Phnom Penh (j): MIKE SHE
Phnom Penh (j): Mac-PDM.09
Ubon (l): MIKE SHE
Ubon (l): SLURP
Ubon (l): Mac-PDM.09
Discharge (% of annual)
J F M A M J J A S O N D
Baseline
1°C
2°C
3°C
4°C
5°C
6°C

Figure 13.